

January 30, 2019

Dear James Roberts,

We have now completed and uploaded responses to the referee comments on our manuscript, "pH-Dependent production of molecular chlorine, bromine, and iodine from frozen saline surfaces," submitted to *Atmospheric Chemistry and Physics*. The referees gave very useful comments, and we feel we have faithfully and completely addressed all the reviewers' concerns. We believe this process has produced a much-improved manuscript, and hope you find this revised paper is now in publishable form.

Sincerely,

John W. Halfacre

### **Response to Anonymous Referee #1**

We would like to thank Anonymous Referee #1 for his/her careful reading of this manuscript and constructive suggestions. We have addressed all of his/her comments in the revised manuscript, and describe in detail changes made below in the order in which they were raised by the reviewer. All page numbers and line numbers are in reference to those in the revised version of the manuscript, except where indicated otherwise. For clarity, the text of the reviewer's comments is in **black**, while the authors' responses are in blue.

**The manuscript by Halfacre et al. describes a number of laboratory experiments conducted to better elucidate the nature of halogen activation from halide-containing ices. This is an important topic in polar boundary layer chemistry, and only a couple of lab studies have been performed on this system before. So there is inherent merit to the work in that regard.**

**The halogen release is driven either by exposure to ozone or by illumination when an OH radical precursor, such as nitrite or hydrogen peroxide, is incorporated into the frozen solution. The experiments are performed using a flow tube that is coupled to a chemical ionization mass spectrometer operated with an iodide reagent ion. The solutions also contain a buffer to maintain the acidity of the solution, given that protons are required for some of these activation processes. I have a few questions concerning the experimental approach (see below) but my major comments are related to the presentation of the experimental results, although I am in general agreement with their interpretations. Some of the results themselves are new and interesting (e.g. I<sub>2</sub> release in the dark) but others have been showed before, albeit with different approaches (e.g. Br<sub>2</sub> release with light).**

**I'll start by saying that I found this paper very challenging to read, especially the Results and Discussion sections which were excessively wordy. The Introduction and Conclusions are fine. Given that there are only a few figures of data, I believe that the experimental results and their discussion could be much more succinctly described, perhaps cut in length by a factor of two. As opposed to describing every observation, could the major findings be emphasized? Indeed, I recommend that the authors rewrite the paper so that the results and associated discussion are united, i.e. the results are discussed as they are presented. I found myself moving back and forth many times between the two sections as I was reading the paper.**

Thank you for your comments and suggestions. We have been diligent in working to improve the readability of the manuscript. The Results and Discussion sections have been combined into Section 3, discussing results as presented, which we believe improved readability, as you suggested. An effort was made to make the new section more concise.

**The Abstract, too, could be improved. For example, the authors should explain what they mean when they state that photochemical production of Br<sub>2</sub> was observed (line 33). What were the conditions that led to Br<sub>2</sub> production?**

We have amended this sentence to clarify that photochemical production of Br<sub>2</sub> at low pH requires an OH precursor (lines 32-33).

**Another example is that the mechanism of the heterogeneous recycling should be mentioned (line 35).**

We have reworded this sentence to clarify that the gas phase HOX compounds would diffuse into our frozen sample solution to oxidize  $X^-$  (line 36)

**Finally, the last sentence should point out that these mechanisms, even if slow, may be important as the initiation of halogen release to the atmosphere, even if it is found they do not ultimately constitute the major source.**

We have included this statement at the end of our abstract (lines ~ 40-43), as suggested.

**Another weakness of the paper is the attempt to connect the laboratory results to those measured in the field. There are so many factors that come into play in this chemistry, I don't think we can plan to quantitatively relate the lab and the field in the manner attempted. For example, is the spatial distribution of the salts, protons, and OH precursors the same in the field snow samples as those in the lab? I believe the answer is no, given the totally different manner by which the ice samples are prepared. For example, how might the buffer materials (such as acetate) interact with OH in the ice? Is the surface segregation of these species the same? My advice would be to give up on the goal of making that comparison, except in the most qualitative manner. My advice would be to give up on the goal of making that comparison, except in the most qualitative manner.**

We have reevaluated our discussion points as a result of this comment and have removed, most notably, the calculation of relative production rates for the field based on our calculated relative reactivities. While we feel the calculation of relative reactivities represents an important empirical result, it is less defensible to apply them quantitatively to field observations derived from samples very different from ours, as the reviewer suggests.

Interactions between buffers and OH are discussed in more detail below under the more specific question from the reviewer. We have also incorporated discussion to this end in the Supplemental Information, lines 3-28.

The reviewer is also correct in implying vast differences in the spatial distribution of ions between our lab samples and field samples. We acknowledge and discuss this point in the paragraph that spans lines 386-407 in the revised manuscript.

**That said, I do believe that the relative rate approach for interpreting the kinetics of oxidation of different halides has merit. There could be more done interpreting these reactivity ratios in terms of the (much better) known bulk aqueous reaction rate constants.**

A comparison of our calculated relative reactivities with the bulk aqueous OH-halide rate constants, along with a discussion of the implications of the differences, has been included and begins on line 372.

### **Experimental questions-**

#### **Will the acetic acid/acetate buffer be affected by volatilization of acetic acid from the ice?**

pH measurements were recorded before and after each experiment, but no statistically significant difference was observed. We have now clarified that this suggests no significant loss of the buffering capacity over the course of the experiment on lines 146-148.

#### **I found line 128 confusing – i.e. was no iodide observed by IC? If so, what LOD was prevalent for the IC method?**

Iodide was not observed above the observed limit of detection by IC. We have clarified this point and added the limit of detection for the method used (90 nM), line 327.

#### **For the bisulfate buffer, will OH react with bisulfate to form the sulfate radical anion, rather than react with the halide ions?**

This reaction pathway will indeed occur, potentially followed by reaction with the halides.



However, the OH reactions rates with the halides are >10,000 faster ( $k_{\text{Cl}^-} = 3 \times 10^9 \text{ M}^{-1} \text{ sec}^{-1}$ ,  $k_{\text{Br}^-} = k_{\text{I}^-} = 1.1 \times 10^{10} \text{ M}^{-1} \text{ sec}^{-1}$ ). We calculate that the sulfate radical would contribute less than 0.1% to halide oxidation, compared that from OH-halide oxidation. Because this is only believed to influence the results to a minor degree, we have included this discussion in the Supplemental Information, lines 3-28.

#### **Line 150: Was it room air that went through the flow tube? If so, what contamination may result?**

The flow tube was cleaned in between experiments with three rinses of ultrapure water with a final rinse of acetone. It was then dried with a > 99.99% purity nitrogen cylinder before being capped. Likely a small amount of room air that contains small amounts of ozone and nitrogen oxides diffuses into the flow tube during the addition of sample to the tube. However, this air would be quickly flushed from the flow tube by zero air on connection with the CIMS, and experimental data are only obtained after signals stabilize. We thank the reviewer for raising this point, and now discuss it on lines 154 as well as detail our cleaning procedure on lines ~181-185.

#### **Line 170: What is the spectrum of the solar simulator bulbs?**

We have included the solar spectrum of the solar simulator bulbs in Figure S1.

**Line 177: typo**

“Ion” was corrected to “Ions”

**Line 189: Where is the Cl<sub>2</sub> background coming from? Just from chloride on flow tube or plumbing surfaces?**

The signal at  $m/z$  197 during ozone addition is not due to Cl<sub>2</sub> because corresponding isotopic signals at  $m/z$  199 and 201 did not rise in concert. This has been clarified in Sect. 2.3, lines 201-203.

**Line 203: I am nervous of how the HOBr sensitivity is estimated, given that the CIMS instrument is not the same as used in the referenced work by Liao et al. Wouldn't it be wiser to just call this signal uncalibrated?**

On line 203-206 of the revisions, we have indicated that the HOBr signal is uncalibrated, and only discuss the relative changes in HOBr signal. Figures 3 and 4 have been adjusted to present the IHOB<sup>-</sup> signals instead of the estimated mole fractions.

## **Response to Anonymous Referee #2**

We would like to thank Anonymous Referee #2 for his/her careful reading of this manuscript and constructive suggestions. We have addressed all of his/her comments in the revised manuscript, and describe in detail changes made below in the order in which they were raised by the reviewer. All page numbers and line numbers are in reference to those in the revised version of the manuscript, except where indicated otherwise. For clarity, the text of the reviewer's comments are in **black**, while the authors' responses are in blue.

**This study reports experiments related to the photochemical halogen release from frozen sea water mimics. The results provide novel information on the halogen oxidation processes and important basis for the interpretation of field data. It becomes apparent that the most important parameters controlling halogen release are the relative proportions of chloride, bromide and iodide, pH and the structure of the frozen system, in terms of the way in which the combination of crystalline ice and brine are exposed to the gas phase. Since there is also a significant debate in the community on especially the latter two, these aspects could also be illuminated a bit better as detailed below. Overall, the experiments have been carefully designed and analysed, and the analysis of the results is associated with a proper discussion of uncertainties and related caveats (e.g., related to molecular chlorine detection in presence of ozone). The careful discussion of the halogen cycling reactions and their kinetics is appreciated. I therefore recommend this study for publication with only a few minor suggestions.**

### **Comments:**

- 1) Since the study also tries to differentiate the relative roles of photochemically produced radicals and ozone for halogen release, I wonder why no experiments have been done with ozone only for reference. While such experiments have been done in the past, indeed, exactly because of the complexity of the system in terms of microstructure, the corresponding 'ozone induced baseline dark halogen release' could have been assessed for comparison.**

Our experiments were inspired by the field work of Pratt et al. (2013) and Raso et al. (2017) that suggested evidence of photochemically-initiated halogen production, the testing of which was the primary focus of this paper. We appreciate the author's comment and acknowledge that such dark experiments with ozone only would have allowed for a more direct comparison of our results with previous laboratory experiments, such as Oum et al. (1998) and Oldridge and Abbatt (2011), discussed in our paper on lines 102-106. However, since Pratt et al. (2013) demonstrated that  $O_3 + Br^-$  was relatively unimportant as a  $Br_2$  source under normal atmospheric  $O_3$  conditions without radiation, we focused on the role of OH as an initiator.

- 2) The authors several times discuss potential surface reactions occurring on liquid brines, I caution that diffusive exchange even over micrometer ranges is very fast, so that all halide ions present in liquid brine are available for reaction. The kinetics may indeed be limited by a surface process, but this is maybe not the important question, because as observed by the authors, it seems rather that the exchange between**

**compartments may be limiting. If brine in a grain boundary is connected to the surface, diffusion is long enough to allow reaction and release within the experimental time scales. Therefore, the question remains where the less available halide ions are, if brine pockets are probably not buried below ice in such thin films. The way the films were frozen, the ice likely started to grow from the Pyrex glass walls.**

We thank the Referee for this comment. The recent work from Malley et al. (2018), cited line 388) discusses the brine distribution in frozen surfaces in much more depth, and we look forward to experiments inspired by this work that will provide further clarity on this issue. But, we expect that the less-available ions are locked in the bulk ice, as discussed in lines 386-407 of the revision.

**3) Could the authors please mention more precisely the irradiation conditions and how they were assessed? Has some actinometry been performed?**

We have reproduced the solar irradiance spectrum of the solar simulator bulbs in Figure S1. No actinometry was performed, but we do not attempt in this paper to simulate the actual ambient radiant fluxes, but rather discuss the relative rates of production, and the roles of pH, and OH and O<sub>3</sub> in the gas phase on those rates.

**4) pH: As the authors mention in the experimental part, this is a challenging aspect. I think a short discussion is adequate there and in the discussion section to emphasize the buffer concentrations used in relation to the halide ions, and in what way this may have affected both the physical properties and the halogen / radical chemistry.**

The hydroxyl radical can react with acetic acid, as well as with bisulfate to form sulfate radical:



However, the OH reactions rates with the halides are considerably faster ( $k_{\text{Cl}^-} = 3 \times 10^9 \text{ M}^{-1} \text{ sec}^{-1}$ ,  $k_{\text{Br}^-} = k_{\text{I}^-} = 1.1 \times 10^{10} \text{ M}^{-1} \text{ sec}^{-1}$ ). We calculate that the sulfate radical would contribute less than 0.1% to halide oxidation, compared that from OH-halide oxidation. Because this is only believed to influence the results to a minor degree, we have included the desired discussion in the Supplemental Information, Lines 3-28.

### **Response to Dr. Bartles-Rausch**

We would like to thank Dr. Bartles-Rausch for his interest in our manuscript and for his comments. We have addressed his comments/questions below in the order in which they were raised. All page numbers and line numbers are in reference to those in the revised version of the manuscript, except where indicated otherwise. For clarity, the text of the Dr. Bartles-Rausch comments is in **black**, while the authors' responses are in blue.

**I read your manuscript with great interest and wish the best for publication in ACP. In particular, I like the increased complexity of your experiments compared to other laboratory studies and the comparison to field data.**

**Would you mind elaborating in more detail where you think the chemistry is occurring in your samples: the liquid fraction or the ice with its disordered interface? You clearly state that the temperature of the sample was above the eutectic of NaCl, so we can expect the presence of liquid in your system.**

Based on the temperature of the experiments, and the ionic strength of the water samples used to make the ice coating, we believe the reactions occur primarily in a liquid brine on the surface of the ice layer and have clarified on lines 158-163, as well as line 2323 of the revised manuscript. This is consistent with Cho et al. (2001) and Oldridge and Abbatt (2011).

**By the way, what would be the volume of liquid compared to that of ice?**

Our experimental sample was 80.0 mL of an Instant Ocean solution that was made to be approximately 0.56 M with respect to NaCl (the most abundant ions in the salt). Based on simple freezing point depression thermodynamics for a 0.56M NaCl solution and an ice  $T = -15^{\circ}\text{C}$ , we calculate a liquid fraction of 0.124.

**Then, later in the discussion the focus is placed on the disordered interface as host of the reactions - as far as I understand the manuscript. I assume you refer to the disordered interface of ice. Could you specify the role of the liquid fraction and of the ice as host for the chemistry? I think at the end this is a semantic issue, as your data are very nicely compared to studies with liquid samples (L. Artiglia, J. Edebeli, F. Orlando, S. Chen, M.-T. Lee, P. Corral Arroyo, A. Gilgen, T. Bartles-Rausch, A. Kleibert, M. Vazdar, M. A. Carignano, J. S. Francisco, P. B. Shepson, I. Gladich and M. Ammann, Nat Comms, 2017, 8, 700.) and to those with frozen samples with a considerable liquid fraction (N. W. Oldridge and J. P. D. Abbatt, J. Phys. Chem. A, 2011, 115, 2590–2598.) Indeed, Oldridge proposed that the reaction occurs in the liquid fraction of their samples.**

For our analysis, we assumed that all of the chemistry occurred in the brine, as indicated on lines 158-163 and 232 of the revised manuscript.

1 **pH-Dependent production of molecular chlorine, bromine, and**  
2 **iodine from frozen saline surfaces**

3 John W. Halfacre<sup>1</sup>, Paul B. Shepson<sup>2,3,4</sup>, Kerri A. Pratt<sup>5</sup>

4 <sup>1</sup>Department of Chemistry, Indiana University Southeast, New Albany, IN USA

5 <sup>2</sup>Department of Chemistry, Purdue University, West Lafayette, IN USA

6 <sup>3</sup>Department of Earth, Atmospheric, and Planetary Sciences, Purdue University, West Lafayette, IN USA

7 <sup>4</sup>School of Marine and Atmospheric Sciences, Stony Brook University

8 <sup>5</sup>Department of Chemistry and Earth & Environmental Sciences, University of Michigan, Ann Arbor, MI USA

9 *Correspondence to:* J. W. Halfacre ([halfacre@ius.edu](mailto:halfacre@ius.edu))

10

11

12

13

14

15

16

17

18

19

20

21

22

23

24

25 **Abstract**

26           The mechanisms of molecular halogen production from frozen saline surfaces remain incompletely  
27 understood, limiting our ability to predict atmospheric oxidation and composition in polar regions. In this laboratory  
28 study, condensed-phase hydroxyl radicals (OH) were photochemically generated in frozen saltwater solutions that  
29 mimicked the ionic composition of ocean water. These hydroxyl radicals were found to oxidize Cl<sup>-</sup>, Br<sup>-</sup>, and I<sup>-</sup>, leading  
30 to the release of Cl<sub>2</sub>, Br<sub>2</sub>, I<sub>2</sub> and IBr. At moderately acidic pH (buffered between 4.5-4.8), irradiation of ice containing  
31 OH-precursors (either of hydrogen peroxide or nitrite ion) produced elevated amounts of I<sub>2</sub>. Subsequent addition of  
32 O<sub>3</sub> produced additional I<sub>2</sub>, as well as small amounts of Br<sub>2</sub>. At lower pH (1.7-2.2) and in the presence of an OH  
33 precursor, rapid dark conversion of I<sup>-</sup> to I<sub>2</sub> occurred from reactions with hydrogen peroxide or nitrite, followed by  
34 substantial photochemical production of Br<sub>2</sub> upon irradiation. Exposure to O<sub>3</sub> under these low pH conditions also  
35 increased production of Br<sub>2</sub> and I<sub>2</sub>; this likely results from direct O<sub>3</sub> reactions with halides, as well as the production  
36 of gas-phase HOBr and HOI that subsequently diffuse to frozen solution to react with Br<sup>-</sup> and I<sup>-</sup>. Photochemical  
37 production of Cl<sub>2</sub> was only observed when the irradiated sample was composed of high-purity NaCl and hydrogen  
38 peroxide (acting as the OH precursor) at pH =1.8. Though condensed-phase OH was shown to produce Cl<sub>2</sub> in this  
39 study, kinetics calculations suggest that heterogeneous recycling chemistry may be equally or more important for Cl<sub>2</sub>  
40 production in the Arctic atmosphere. The condensed-phase OH-mediated halogen production mechanisms  
41 demonstrated here are consistent with those proposed from recent Arctic field observations of molecular halogen  
42 production from snowpacks. These reactions, even if slow, may be important for providing seed halogens to the Arctic  
43 atmosphere. Our results suggest the observed molecular halogen products are dependent on the relative concentrations  
44 of halides at the ice surface, as we only observe what diffuses to the air-surface interface.

45

46

47

## 48 1 Introduction

49 It is now well-established that gas-phase halogen species influence atmospheric composition through reactions  
50 with ozone (O<sub>3</sub>), volatile organic compounds (VOCs), and gaseous elemental mercury (Hg<sup>0</sup>) (Barrie and Platt, 1997;  
51 Carpenter et al., 2013; Platt and Hönninger, 2003; Saiz-Lopez and von Glasow, 2012; Simpson et al., 2007, 2015;  
52 Steffen et al., 2008, 2014, and references therein). In polar regions, it is believed that halogens build up to effective  
53 concentrations through a heterogeneous reaction sequence known as the “halogen explosion” (Reactions R1-4, where  
54 X represents Cl, Br, or I) (Garland and Curtis, 1981; Tang and McConnell, 1996; Vogt et al., 1996; Wennberg, 1999).



59 In this sequence, a molecular halogen (X<sub>2</sub>) is photolyzed to produce two reactive halogen radicals. These radicals can  
60 react with O<sub>3</sub> to produce halogen oxides (XO). The XO produced in Reaction R2 rapidly photolyzes (or reacts with  
61 NO) to regenerate O<sub>3</sub> and X<sub>2</sub> in a null cycle. To irreversibly remove ambient O<sub>3</sub>, XO must react with another halogen  
62 oxide or Hg<sup>0</sup>. Alternatively, XO can react with HO<sub>2</sub> to form HOX (Reaction R3) or NO<sub>2</sub> to form XONO<sub>2</sub>. Gas-phase  
63 HOX can heterogeneously react with salt-laden surfaces, including sea-salt aerosol particles (McConnell et al., 1992)  
64 and the “disordered interface” (often referred to as a quasi-liquid or quasi-brine layer) that exists on frozen saline  
65 surfaces (Bartels-Rausch et al., 2014; Cho et al., 2002) to produce X<sub>2</sub>, effectively returning two halogen radicals to  
66 the gas phase. Additionally, this mechanism is enhanced under acidic conditions, confirmed by laboratory studies of  
67 aqueous (Fickert et al., 1999) and frozen solutions (e.g., Abbatt et al., 2010; Sjostedt and Abbatt, 2008; Wren et al.,  
68 2013), and from field observations (Pratt et al., 2013).

69 While much has been learned about the atmospheric chemistry of reactive halogen species in the Arctic,  
70 knowledge gaps remain in the chemical mechanisms by which molecular halogens are produced from frozen surfaces  
71 (Liao et al., 2014; Pratt et al., 2013). Recently, in situ, light-induced production of Cl<sub>2</sub> (Custard et al., 2016), Br<sub>2</sub> (Pratt  
72 et al., 2013; Raso et al., 2017), and I<sub>2</sub> (Raso et al., 2017) within snowpack interstitial air has been reported, and was  
73 further demonstrated to be enhanced following the addition of O<sub>3</sub>. The Br<sub>2</sub>-producing snowpacks studied by Pratt et  
74 al. (2013) were characterized as having larger surface area, lower pH (≤ 6.3), greater [Br<sup>-</sup>]/[Cl<sup>-</sup>] molar ratios (≥ 1/148),

75 and lower salinity relative to other frozen samples collected near Utqiagvik, Alaska. The proposed mechanism for this  
76 chemistry is based on laboratory studies of condensed-phase, hydroxyl radical (OH)-mediated halogen oxidation  
77 (Reactions R5-R12), that is followed by partitioning of the molecular halogen to the gas phase (Abbatt et al., 2010;  
78 Knipping et al., 2000; Oum et al., 1998b).



87 Direct, light-induced halogen production from frozen surfaces in the presence of OH has been previously demonstrated  
88 in the laboratory for Br<sub>2</sub> and possibly for I<sub>2</sub> (Abbatt et al., 2010), but analogous chemistry for Cl<sub>2</sub> has yet to be observed.  
89 Additionally, photochemical production of I<sub>2</sub> has been directly observed in the absence of OH (Kim et al., 2016).  
90 Employing cavity ring-down spectroscopy, Kim et al. (2016) reported photochemical production of I<sub>2</sub> from a frozen  
91 solution by known aqueous-phase chemistry (R13-17). This proposed photochemical mechanism involves an (I-O<sub>2</sub>)  
92 charge-transfer complex (Levanon and Navon, 1969).



98 Kim et al. (2016) also report enhanced photochemical I<sub>3</sub><sup>-</sup> production (determined spectrophotometrically) from sunlit  
99 frozen iodide solutions placed on Antarctic snowpack, as well as from refrozen field snow and glacier samples doped

100 with iodide. A question is thus raised regarding the necessity of OH for I<sub>2</sub> production under environmentally-relevant  
101 conditions.

102 The role of O<sub>3</sub> in halogen production on frozen surfaces is also unclear. Previous laboratory studies have  
103 demonstrated that halide-doped frozen surfaces exposed to O<sub>3</sub> can lead to Br<sub>2</sub> production (independent of radiation,  
104 R18-R19, and R4) (Oldridge and Abbatt, 2011; Oum et al., 1998a; Wren et al., 2013).



107 It has recently been shown that this process proceeds at the surface, through a water-stabilized ozonide, Br·OOO<sup>-</sup>, as  
108 shown in reactions R20-R22. Artiglia et al. (2017) observed this Br·OOO<sup>-</sup> intermediate via liquid-injection X-ray  
109 photoelectron spectroscopy.



113 Wren et al. (2013) found that Cl<sub>2</sub> was produced primarily via heterogeneous recycling of HOCl, resulting from BrCl  
114 photolysis, on halide-rich artificial snow. However, the observation that O<sub>3</sub> induces halogen production from natural  
115 frozen surfaces has yet to be confirmed by field observations of snowpack chemistry, in which exposure to only O<sub>3</sub> in  
116 the absence of light has not been shown to produce molecular halogens (Custard et al., 2017; Pratt et al., 2013; Raso  
117 et al., 2017). This raises a question of whether O<sub>3</sub> is more important for initial halogen release, or in a gas phase  
118 propagation/recycling capacity (i.e., per the halogen explosion).

119 In this study, we utilized a custom ice-coated-wall flow reactor in tandem with chemical ionization mass  
120 spectrometry (CIMS) to study Br<sub>2</sub>, Cl<sub>2</sub>, and I<sub>2</sub> production from frozen surfaces with compositions mimicking sea ice.  
121 The effects of photochemically generated OH radicals, O<sub>3</sub> addition, and pH are tested as they relate to the production  
122 of these halogens. Surface pH was controlled through use of buffers.

123 2 **Methods**

124 **2.1 Materials**

125 Sample solutions were composed to mimic the halide composition of seawater. This was achieved using  
126 either dissolved Instant Ocean (Spectrum Brands), or commercially available halide salts at a composition that mimics  
127 Instant Ocean (for consistency) in solutions referred to hereafter as “saltwater.” The halide concentrations in these  
128 solutions were made to a final concentration of 0.56M Cl<sup>-</sup>, 7.2 x 10<sup>-4</sup> M Br<sup>-</sup>, and 1.9 x 10<sup>-6</sup> M I<sup>-</sup>. Except for Instant  
129 Ocean, all chemicals were purchased from Sigma Aldrich. Halide salts include solid NaCl (puriss. p.a. grade, ≥99.5%  
130 purity), NaBr (puriss. grade, >99% purity), KI (puriss. p.a. grade, ≥99.5% purity). We note that these halide  
131 concentrations are comparable to those in actual seawater (Herring and Liss, 1974; Luther et al., 1988; Tsunogai and  
132 Sase, 1969), which typically contains Cl<sup>-</sup>, Br<sup>-</sup>, and I<sup>-</sup> at ratios of 1:<sup>1/660</sup>:<sup>1/200,000</sup>. Solutes were dissolved in ultrapure  
133 water (Birck Nanotechnology Center). Dissolved organic carbon for Instant Ocean and halide salt solutions were  
134 analyzed using a Shimadzu TOC-V<sub>CSH</sub> Total Organic Carbon Analyzer, and determined at approximately 70 mg/L for  
135 Instant Ocean solutions, and less than 5 mg/L for saltwater solutions. No further characterization of carbon-containing  
136 compounds was performed.

137 While previous investigators have adjusted the pre-freezing pH of their samples, it is very difficult to know  
138 the pH in the surface brine (or disordered interface) of frozen samples (Bartels-Rausch et al., 2014), though there is  
139 evidence from laboratory studies suggesting that the pH of salt solutions remains largely unchanged after freezing  
140 (Wren and Donaldson, 2012b). To obviate this problem, the aqueous solutions used in this study were buffered so  
141 that the same pH should exist in the surface brine layer. All solutions were buffered by either a 20 mM acetic acid  
142 (ACS reagent grade, ≥99.7% purity)/acetate (puriss. p.a. grade) buffer (pH ≈ 4.5-4.7), or a 20 mM bisulfate  
143 (ReagentPlus grade, 99% purity)/sulfate (ReagentPlus grade, ≥ 99.0% purity) buffer (pH ≈1.7 – 2.2). These buffer  
144 concentrations were chosen as a compromise between using as little buffer as possible, yet enough buffer to ensure  
145 adequate buffering ability, as buffer capacity rapidly decreases as constituent species concentrations approach the acid  
146 K<sub>a</sub> value. pH values of sample solutions were determined before and after experiments with no significant changes  
147 observed, suggesting the buffer composition/buffering capacity does not appreciably change over the course of an  
148 experiment (discussed further in the Supplemental Information). 100 μM of either hydrogen peroxide (trace analysis

149 grade,  $\geq 30\%$  purity) or sodium nitrite (ReagentPlus grade,  $\geq 99.0\%$  purity) were included as photochemical hydroxyl  
150 radical precursors, via reactions R5, and R6-7.

## 151 2.2 Flow tube

152 Experiments were performed in a custom-built 150 cm long, 2.5 cm ID frozen-walled Pyrex flow tube  
153 contained within a temperature-controlled cooling jacket. In each experiment, 80.0 mL of sample solution was poured  
154 into the tube **in the presence of room air**, which was subsequently sealed with vinyl caps (McMaster-Carr). The flow  
155 tube was then rotated on motorized rollers within a 170 cm x 50 cm x 50 cm, insulated wooden cooling chamber.  
156 Crushed dry ice was placed along the bottom of the chamber, and fans were used to circulate the air throughout the  
157 chamber such that the flow tube was evenly cooled. After  $\sim 30$  minutes, the sample was evenly frozen (ice thickness  
158 of 0.9 mm). The flow tube was subsequently transferred to an enclosed 156 cm x 50 cm x 50 cm wooden, Mylar-  
159 lined experiment chamber, and connected to a recycling chiller set to 258 K (i.e., above the  $\text{NaCl}\cdot 2\text{H}_2\text{O}$  eutectic point,  
160 in which the relevant chemical reactions are expected to occur with / in a brine on the ice surface (Cho et al., 2002;  
161 Oldridge and Abbatt, 2011)). This conjecture is based on the work of Oldridge and Abbatt (2011), who reported from  
162 a series of similar experiments that when  $\text{O}_3$  is flowed over frozen  $\text{NaCl}/\text{NaBr}$  solutions above the  $\text{NaCl}$  eutectic  
163 temperature, reaction kinetics were strongly consistent with chemistry occurring in a liquid brine. The cooling liquid  
164 used for the chiller was a mixture of 60% ethylene glycol and 40% distilled water. Six UVA-340 solar simulator  
165 lamps (Q-Lab, 295 – 400 nm with maximum wattage at 340 nm, **irradiance spectrum in Fig. S1**) were installed in the  
166 experiment box (two on each side except bottom). Each side was lined with reflective Mylar sheets to evenly irradiate  
167 the flow tube when the lamps were powered.

168 A flow schematic representing typical experiments is shown in Fig. 1. The carrier gas (Air, Ultra Zero grade,  
169 Praxair) was scrubbed of volatile organic compounds using activated charcoal, and water by travelling through coiled  
170 stainless-steel tubing surrounded by crushed dry ice (replaced throughout the course of an experiment). This gas was  
171 measured to contain  $\leq 300 - 400 \text{ pmol mol}^{-1}$  NO (experimentally determined limits of detection) using the Total  
172 REactive Nitrogen Instrument (TRENI) (Lockwood et al., 2010; Xiong et al., 2015). Though  $\text{NO}_2$  was not measured,  
173 it should have been removed by the charcoal trap. Before entering the coated-wall flow tube, the carrier gas flowed  
174 through a commercial  $\text{O}_3$  generator (2B Technologies model 306). Carrier gas air entered the tube near room  
175 temperature (20 °C). At the start of experiments, the  $\text{O}_3$  generator was set to  $0 \text{ nmol mol}^{-1}$ . Carrier gas then entered

176 the flow tube in the dark experiment chamber. In most experiments, the carrier gas was regulated to a volumetric flow  
177 rate of 4.0 L min<sup>-1</sup>, which yields a residence time in the flowtube of ~12 seconds. On exiting the flow tube, sample  
178 air was characterized using a Thermo Environmental 49i O<sub>3</sub> monitor (flow rate of ~1.5 L min<sup>-1</sup>) and a chemical  
179 ionization mass spectrometer (CIMS, sampling flow rate of ~1.7 L min<sup>-1</sup>, described below in Sect 2.3). Excess flow  
180 air was vented away. At set times in an experiment, the solar simulator bulbs were activated, and O<sub>3</sub> was added to the  
181 system by powering the O<sub>3</sub> generator. At the end of each experiment, the ice was melted and the water collected for  
182 pH measurements. To clean the flow tube, its interior was washed three times with ultrapure water before a final rinse  
183 with wash acetone. The flow tube was then connected to a compressed nitrogen gas cylinder (Praxiar, >99.99% purity)  
184 to dry for at least 2 hours. Once dry, the flow tube was disconnected and capped until the next experiment.

### 185 2.3 CIMS

186 Halogen species were detected using a chemical ionization mass spectrometer (CIMS), described previously  
187 by Liao et al. (2011) and Pratt et al. (2013). Chemical ionization is achieved by ion-molecule reactions that occur  
188 between iodide-water reagent clusters, I(H<sub>2</sub>O)<sub>n</sub><sup>-</sup> in N<sub>2</sub>, and the gas-phase analytes in zero air. The iodide-water clusters  
189 are formed when gas-phase iodide ions, generated by flowing 5 ppm methyl iodide through a <sup>210</sup>Po ionizer (NRD)  
190 combines with water in the humidified ion-molecule region of the CIMS. Ion were filtered using a quadrupole mass  
191 filter. The ice-coated flowtube was connected to the CIMS via approximately 50 cm of i.d. 1/2" PFA Teflon tubing.

192 A typical CIMS sampling cycle consisted of an 8.35s duty cycle. Dwell times for all monitored species were  
193 250 ms except for the reagent ion (detected as *m/z* 147, I(H<sub>2</sub><sup>18</sup>O)<sup>-</sup>), which was set to a dwell time of 100 ms. The 18  
194 ions analyzed in this study are listed in Table 1, but we focus herein on results concerning masses related to Br<sub>2</sub> (*m/z*  
195 285 and 287: I<sup>79</sup>Br<sup>79</sup>Br<sup>-</sup> and I<sup>81</sup>Br<sup>79</sup>Br<sup>-</sup>, respectively), Cl<sub>2</sub> (*m/z* 197, 199, and 201: I<sup>35</sup>Cl<sup>35</sup>Cl<sup>-</sup>, I<sup>37</sup>Cl<sup>35</sup>Cl<sup>-</sup>, and I<sup>37</sup>Cl<sup>37</sup>Cl<sup>-</sup>),  
196 and I<sub>2</sub> (*m/z* 381: I<sub>3</sub><sup>-</sup>). In addition, IBr (*m/z* 333 and 335: I<sup>79</sup>IBr<sup>-</sup>, I<sup>81</sup>IBr<sup>-</sup>) was unambiguously detected in some  
197 experiments. The presence of Br<sub>2</sub>, Cl<sub>2</sub>, and IBr was confirmed by measuring the ratios between the two isotope signals  
198 for each mass, compared to the natural abundances (i.e., 1.95 for *m/z* 287:285; 1.54 for *m/z* 197:199; and 1.03 for *m/z*  
199 333:335, respectively). Data outside ±25% the expected isotope ratio were excluded from analysis. The signals for  
200 BrCl (*m/z* 241 and 243: I<sup>79</sup>Br<sup>35</sup>Cl<sup>-</sup>, I<sup>81</sup>Br<sup>35</sup>Cl<sup>-</sup>, I<sup>79</sup>Br<sup>37</sup>Cl<sup>-</sup>) masses were never observed at the correct ratios (1.3 for *m/z*  
201 243:241), and so those data were not reported here. As the introduction of ~60 nmol mol<sup>-1</sup> O<sub>3</sub> to the experimental  
202 system significantly increased the baseline signal of *m/z* 197, but not *m/z* 199 or 201, the presence of Cl<sub>2</sub> could not be

203 confirmed under elevated O<sub>3</sub> conditions. In addition, background subtracted, relative signals for *m/z* 271 (IHOI) and  
204 *m/z* 225 (IHO<sup>81</sup>Br<sup>-</sup>) are discussed (signals are relative to that of the ionization gas (*m/z* 147, I(H<sub>2</sub><sup>18</sup>O))). According to  
205 isotope ratios, IHOBr<sup>-</sup> was not unambiguously observed, however, due to an interference at *m/z* 223 (IHO<sup>79</sup>Br<sup>-</sup>), and  
206 our results here should be considered for only qualitative purposes as we only discuss relative changes in the signal.

207 CIMS calibrations were performed using I<sub>2</sub>, Br<sub>2</sub>, and Cl<sub>2</sub> permeation devices (VICI) at the start and  
208 conclusion of each experiment. Br<sub>2</sub> and Cl<sub>2</sub> permeation outputs were quantified using the spectrophotometric method  
209 described by Liao et al. (2012). The I<sub>2</sub> permeation output was quantified by flowing the I<sub>2</sub> through an impinger  
210 containing a NaHCO<sub>3</sub> (30mM)/NaHSO<sub>3</sub> (5mM) reducing solution. This solution quantitatively reduces I<sub>2</sub> to I<sup>-</sup>, which  
211 was then determined using a Dionex DX500 ion chromatography system. Permeation rates were calculated for each  
212 experiment and found to average (1.9±0.1) × 10<sup>-11</sup>, (5.5±0.1) × 10<sup>-10</sup>, and (8.6±0.1) × 10<sup>-10</sup> mol min<sup>-1</sup> of I<sub>2</sub>, Br<sub>2</sub>, and  
213 Cl<sub>2</sub>, respectively (uncertainties representing standard error of the mean). CIMS calibration factors were calculated for  
214 individual experiments. These factors are based on the average of the signal sensitivities, determined from the  
215 permeation sources, calculated at the start and completion of each experiment. Corresponding uncertainties for these  
216 calibration factors thus represent the 1σ standard deviation of the mean sensitivity. An approximate I<sup>79</sup>IBr<sup>-</sup> calibration  
217 factor was assumed to be the average of the sensitivities for *m/z* 287 (IBr<sub>2</sub><sup>-</sup>) and 381 (I<sub>3</sub><sup>-</sup>). Background measurements  
218 were performed before and after the experiment (minimum of 5 min) by passing the carrier gas through the  
219 experimental flow tube (without O<sub>3</sub>, in the dark), and subsequently through a glass wool scrubber, previously shown  
220 to remove molecular halogens with greater than 95% efficiency (Liao et al., 2012; Neuman et al., 2010). Temporal  
221 variations in bromine-species signals while using the low pH sulfate/bisulfate buffer were observed in some  
222 experiments (Fig. S2) and are discussed in the Supplementary Information.

223 Analysis of experimental data was based on one-minute averages, with uncertainties representing the  
224 standard deviation of these averages. Subsequently, signals were converted to concentrations using the sensitivities  
225 calculated above, propagating the sensitivity uncertainty into the measurement uncertainty. Average limits of  
226 detection (3σ) across all experiments for the molecular halogens during background periods were 1.8 ± 0.4, 1.2 ± 0.3,  
227 and 9 ± 2 pmol mol<sup>-1</sup> for Br<sub>2</sub>, Cl<sub>2</sub>, and I<sub>2</sub> respectively (uncertainties representing standard error of the mean).  
228 Additionally, reported uncertainties for integrated amounts of formed halogens are calculated as integrated halogen  
229 concentrations multiplied by the relative uncertainty in the CIMS signal sensitivity.

### 230 3 Results and Discussion

231 The experiments described here address the extent to which condensed-phase OH radicals **in an ice surface brine**  
232 (Cho et al., 2002) can produce I<sub>2</sub>, Br<sub>2</sub>, and Cl<sub>2</sub> through condensed-phase reactions within frozen saline surfaces, as  
233 hypothesized by recent field (Custard et al., 2017; Pratt et al., 2013; Raso et al., 2017) and laboratory experiments  
234 (Abbatt et al., 2010). In addition, we test the pH-dependence of this chemistry and whether gas-phase O<sub>3</sub> enhances  
235 this production. We find the relative and absolute amounts of halogens produced from ice are a complex function of  
236 the relative concentrations of the precursor halide ions, pH, presence of oxidants, radiation, and O<sub>3</sub>.

237 The ice-coated flow tube experiments started under dark conditions and without addition of O<sub>3</sub> (Sect. 3.1). Once  
238 signals stabilized, lights were activated (Sect. 3.2). After 1-2 hours, ~60 nmol mol<sup>-1</sup> of O<sub>3</sub> was introduced into the  
239 carrier gas (Sect. 3.3). Integrated amounts of produced molecular halogens are presented in Table 2 for all  
240 experiments. Unless otherwise specified, integrated amounts of produced halogens represent amounts produced over  
241 the course of 1 h of exposure to light (Sect. 3.2) and/or ozone (Sect. 3.3). Saline ices tested include frozen Instant  
242 Ocean (IO) solutions, “saltwater” (SW) solutions composed of dissolved reagent grade salts mimicking seawater  
243 composition, and 0.56 M high purity NaCl (CL1). OH-radical precursors used include hydrogen peroxide (H<sub>2</sub>O<sub>2</sub>) or  
244 nitrite (NO<sub>2</sub><sup>-</sup>), which have been estimated to account for 96% of snowpack photochemical OH formation at Utqiagvik,  
245 AK (France et al., 2012). Many of the salient features of our results are demonstrated by example experiments shown  
246 in Fig. 2, including the impact of irradiation in the presence of ice phase OH radical precursors, varied pH, and the  
247 presence of O<sub>3</sub>. Below we discuss the results and interpretations of our experiments, organized by the mechanism of  
248 halogen production and halogen products themselves.

#### 249 3.1 Dark reaction production of I<sub>2</sub>

250 After the initial connection of the flowtube to the CIMS (i.e., before irradiation or addition of O<sub>3</sub>), large I<sub>2</sub>  
251 signals (measured as I<sub>3</sub><sup>-</sup>, *m/z* 381) were observed in several cases where OH-radical precursors were utilized, especially  
252 when pH ≤ 2 (e.g., Fig. 2b, Fig. S2). Integrated calibrated sums of this dark I<sub>2</sub> production are estimated in Table S1,  
253 and span from the time when the flowtube was connected to the CIMS until lights were activated. When pH ≤ 2, dark  
254 production of I<sub>2</sub> sometimes caused significant depletion of reservoir I<sup>-</sup>. Experiments IO4 and SW5 (both using H<sub>2</sub>O<sub>2</sub>  
255 as an OH precursor) only had, at most, ~36% of the initial 152 nmol of I<sup>-</sup> by the time lights were turned on (remaining  
256 I<sup>-</sup> was estimated by subtracting twice the observed I<sub>2</sub> (i.e., two I<sup>-</sup> for every I<sub>2</sub>) from the initial 152 nmol of I<sup>-</sup> in the IO

257 or SW solutions). Considerably less dark I<sub>2</sub> production occurred using NO<sub>2</sub><sup>-</sup> as an OH precursor (depleting I<sup>-</sup> by an  
258 average of 4.5%, Table S1). However, the amounts in Table S1 represent lower limits of the dark-produced I<sub>2</sub>; it is  
259 impossible to accurately determine the extent of dark I<sub>2</sub> production since some was lost from the flow tube during its  
260 connection to the CIMS after freezing (Fig. 1). At pH ≈ 4.7, this production was relatively modest. Only experiment  
261 IO2 was noticeably affected, in which only ~0.5% of initial I<sup>-</sup> was removed by dark mechanisms (Table S1). Under  
262 both pH regimes (i.e. ~4.7 and < 2), this signal subsequently decayed as I<sub>2</sub> flushed out of the system until reaching a  
263 low steady state concentration. No corresponding dark production of Br<sub>2</sub> or Cl<sub>2</sub> was observed for any experiments at  
264 any pH.

265 As previously reported, both H<sub>2</sub>O<sub>2</sub> and NO<sub>2</sub><sup>-</sup> can directly convert I<sup>-</sup> to I<sub>2</sub> under dark acidic conditions. The  
266 oxidation of I<sup>-</sup> by H<sub>2</sub>O<sub>2</sub> occurs through the condensed phase reactions R23 and R24 (Küpper et al., 1998):



269 Nitrite ions react with hydronium ions to form the nitroacidium ion, H<sub>2</sub>ONO<sup>+</sup>, which has been previously shown to  
270 produce I<sub>2</sub> (R25-R27) (Hellebust et al., 2007; O'Driscoll et al., 2006, 2008; O'Sullivan and Sodeau, 2010):



274 Therefore, it is likely the I<sub>2</sub> observed on connection of the flowtube to CIMS originated from the above reactions  
275 (R23-27), as the pH ≤ 2 experiments in this work (IO3-5, SW3-5) favor these forward reactions.

## 276 **3.2 Hydroxyl radical-induced halogen production**

### 277 **3.2.1 pH ≈ 4.7**

278 At pH ≈ 4.7, frozen solutions without OH radical precursors produced no (IO6, SW6-SW7) or little (IO7,  
279 0.10 ± 0.06 nmol of I<sub>2</sub>) amounts of molecular halogens above their respective LODs after activation of lights (Table  
280 2). The small amount of I<sub>2</sub> produced in IO7 possibly originates from the light and O<sub>2</sub>-mediated production mechanism  
281 proposed by Kim et al. (2016) as summarized within R13-R17. However, as shown below, this mechanism of I<sub>2</sub>  
282 production is of relatively minor importance at this pH.

283 In the presence of  $\text{H}_2\text{O}_2$  at  $\text{pH} \approx 4.7$ ,  $\text{I}_2$  mole fractions increased rapidly upon irradiation, as shown in Fig. 2a.  
284 Of the four experiments performed in these conditions (IO1, IO2, SW1, SW2), three experiments (IO1, SW1, SW2)  
285 produced statistically similar amounts of  $\text{I}_2$  (mean:  $8 \pm 2$  nmol) after one hour of irradiation (Table 2). The  $\text{I}_2$  signal  
286 behavior in Experiment IO2 qualitatively shared the same features as Experiments IO1, SW1, and SW2 (Fig. S3), but  
287 provided an apparently statistically different amount of  $\text{I}_2$  ( $0.6 (\pm 0.4)$  nmol) based on the objectively chosen integration  
288 limits. This experiment is discussed further in the Supplemental Information.

289 Regarding other molecular halogens, IBr was observed above the estimated limits of detection ( $3$  pmol  
290  $\text{mol}^{-1}$ ) upon irradiation during Experiment SW2 (Fig. 2a), starting approximately 20 minutes before the addition of  
291  $\text{O}_3$ . No photochemically produced (OH-induced)  $\text{Br}_2$  was unambiguously observed at this pH (note that the apparent  
292 IO2  $\text{Br}_2$  production of  $0.034 \pm 0.003$  nmol is likely overestimated and discussed in more detail in the Supplemental  
293 Information).  $\text{Cl}_2$  mole fractions remained below limits of detection in all cases with OH-precursors at this pH.

### 294 3.2.2 $\text{pH} \leq 2$

295 In cases without OH precursors at  $\text{pH} \leq 2$ , photochemical  $\text{I}_2$  production was observed (integrated production  
296 of  $14 \pm 10$  nmol for IO8, and  $6 \pm 2$  nmol for SW8) (Table 2), contrasting with experiments performed at  $\text{pH} \approx 4.7$  in  
297 which very little was produced. This production likely stems from the mechanisms outlined by Kim et al. (2016)  
298 (R13-17), which requires only light and oxygen to form a charge-transfer complex that results in  $\text{I}_2$  production  
299 (discussed in Sect. 1). Molecular  $\text{Br}_2$  and  $\text{Cl}_2$  concentrations remained below limits of detection, consistent with  
300 Abbatt et al. (2010), in which no  $\text{Br}_2$  or  $\text{Cl}_2$  was observed without an OH-precursor.

301 As discussed in Sect. 3.1, inclusion of  $\text{H}_2\text{O}_2$  or  $\text{NO}_2^-$  can result in direct oxidation of  $\text{I}^-$  and reduce the available  
302  $[\text{I}^-]$  for photochemical OH oxidation when  $\text{pH} \leq 2$ . Photochemical production of  $\text{I}_2$  across experiments yielded  $\leq 0.82$   
303 nmol (IO4, IO5, and SW5) when  $\text{H}_2\text{O}_2$  was used as an OH precursor. However, when instead  $\text{NO}_2^-$  was used (as in  
304 IO3, SW3, and SW4), initial observations of  $\text{I}_2$  on flowtube connection to CIMS were as much as 90% less than when  
305  $\text{H}_2\text{O}_2$  was used (Table S1), thereby leaving more  $\text{I}^-$  available for reaction. For experiment IO3 (using  $\text{NO}_2^-$ ), the  
306 reduced pH led to an observed photochemical  $\text{I}_2$  production amount of  $39 \pm 1$  nmol, approximately four times larger  
307 than the largest amount observed at  $\text{pH} \approx 4.7$  ( $9 \pm 3$  nmol, Table 2). That production would be enhanced at lower pH  
308 was expected based on the halogen activation reactions R4-R22. The corresponding “saltwater” experiments using  
309  $\text{NO}_2^-$  were not as conclusive; experiment SW3 only yielded  $4.0 \pm 0.1$  nmol of photochemical  $\text{I}_2$  (Fig. S5). Experiment

310 SW4 (a repeat of SW3) did not produce any photochemical I<sub>2</sub> and qualitatively resembles the H<sub>2</sub>O<sub>2</sub> experiments  
311 performed at this pH. It is possible that, for SW3 and SW4, more I<sub>2</sub> was produced by dark reactions and flushed out  
312 of the tube during connection with the CIMS and therefore would not have been measured.

313 Photochemical production of Br<sub>2</sub> does not appear until I<sub>2</sub> production decreases. The results shown in Figures  
314 2a and 2b demonstrate that when [I<sup>-</sup>]/[Br<sup>-</sup>] approximates the initial conditions of Instant Ocean (~2.6 x 10<sup>-3</sup>), OH-  
315 mediated I<sub>2</sub> production precedes Br<sub>2</sub> and IBr production (as in the pH ≈ 4.7 experiments and IO3, in which significant  
316 dark I<sub>2</sub> production was not observed). After [I<sup>-</sup>]/[Br<sup>-</sup>] has sufficiently decreased, Br<sub>2</sub> eventually becomes the dominant  
317 photochemical product. As demonstrated by experiment IO4 (Fig 2b and inset), there is a delay in Br<sub>2</sub> production  
318 until I<sup>-</sup> was removed as I<sub>2</sub>, then as IBr. For experiments that used H<sub>2</sub>O<sub>2</sub>, photochemical Br<sub>2</sub> yields averaged 4.5 ± 0.5  
319 nmol between IO4 and IO5, and 6.0 ± 0.7 nmol from SW5. Experiment SW4 (using NO<sub>2</sub><sup>-</sup>) produced a comparable  
320 amount of Br<sub>2</sub> (5.4 ± 0.7 nmol). Given the initial depletion of I<sup>-</sup> from dark I<sub>2</sub> production (Sect. 3.1), we can estimate  
321 [I<sup>-</sup>]/[Br<sup>-</sup>] at pH ≤ 2 in ice with H<sub>2</sub>O<sub>2</sub> just before irradiation based on the remaining moles of I<sup>-</sup> in solution (Table S1)  
322 and the total moles of Br<sup>-</sup> in the solution. Averaging values from Experiments IO4-5 and SW5, [I<sup>-</sup>]/[Br<sup>-</sup>] was calculated  
323 as (1.6 ± 0.7) x 10<sup>-4</sup> (compared to the initial ratio of 2.6 x 10<sup>-3</sup>) and was sufficiently low to result in photochemical  
324 production of Br<sub>2</sub>.

325 Photochemical Cl<sub>2</sub> production was only observed from a frozen solution of “pure” 0.56 M NaCl and H<sub>2</sub>O<sub>2</sub> at  
326 pH=1.8 (CL1), as shown in Fig. 2c. The initial Br<sup>-</sup> impurity of this CL1 solution was determined to be (4.5 ± 0.3) x  
327 10<sup>-6</sup> M via ion chromatography, while any I<sup>-</sup> impurity concentration could not be detected above the 3σ LOD of 90  
328 nM. When the lights were turned on, slight increases in I<sub>2</sub> and IBr were observed in concert with a rapid rise in Br<sub>2</sub>.  
329 After about one hour of apparent equilibrium, I<sub>2</sub> concentrations began decreasing, while Br<sub>2</sub>, IBr, and Cl<sub>2</sub> continued  
330 rising. Over one hour of illumination, 93 ± 3 pmol of Cl<sub>2</sub>, 100 ± 10 pmol of Br<sub>2</sub>, and 100 ± 10 pmol of I<sub>2</sub> were observed.  
331 However, as shown in Fig 2c, the greatest rate of increase in Cl<sub>2</sub> signal occurred just after this time. Integrating instead  
332 from t=0 until t=2 hours, the amount of Cl<sub>2</sub> produced was 190 ± 10 pmol, while the amount of Br<sub>2</sub> increased to 310 ±  
333 20 pmol. Utilizing the starting halide concentrations of Br<sup>-</sup> and Cl<sup>-</sup> for CL1, our results show Cl<sub>2</sub> production was  
334 observed at [Br<sup>-</sup>]/[Cl<sup>-</sup>] of 8.1 x 10<sup>-6</sup> (1/124,000), compared to the Instant Ocean [Br<sup>-</sup>]/[Cl<sup>-</sup>] of ~ 1/800. Unfortunately, BrCl  
335 could not be observed due to an unknown interference at m/z 241 and 243.

336 The observations in this study indicate competition for the OH radical in which the most oxidizable halide is  
337 oxidized, and the corresponding molecular halogens are produced until that halide ion is depleted in the ice surface

338 brine reaction environment. The trends in molecular halogen production confirm acid-enhanced mechanisms in which  
 339 the dominant products are largely dependent on relative halide ratios. Here, Br<sub>2</sub> and IBr were not observed until I<sub>2</sub>  
 340 production sufficiently decreased the [I<sup>-</sup>]/[Br<sup>-</sup>] ratio, and Cl<sub>2</sub> was not observed unless the [Br<sup>-</sup>]/[Cl<sup>-</sup>] ratio was  
 341 sufficiently low ([Br<sup>-</sup>]/[Cl<sup>-</sup>] = 8.1 x 10<sup>-6</sup>, as discussed above). This observation is consistent with Sjostedt and Abbatt  
 342 (2008), who exposed frozen salt solutions to gas-phase OH and found peak BrCl production occurred as Br<sup>-</sup> decreased  
 343 from an initial [Br<sup>-</sup>]/[Cl<sup>-</sup>] of 7.3 x 10<sup>-5</sup>. Additionally, Abbatt et al. (2010) generated condensed phase OH on frozen  
 344 surfaces via the photolysis of nitrate, and similarly found lower Br<sub>2</sub> and IBr integrated amounts at lower [Br<sup>-</sup>]/[Cl<sup>-</sup>]  
 345 when temperatures were higher than the eutectic point of sodium chloride. These halide ratios are also consistent with  
 346 in situ snowpack observations of Br<sub>2</sub>, BrCl, and Cl<sub>2</sub> formation (Custard et al., 2017; Pratt et al., 2013).

### 347 **3.2.3 Relative Reactivities of OH-induced Halogen Production**

348 I<sub>2</sub>, Br<sub>2</sub>, and Cl<sub>2</sub> have been previously observed at mole fractions within less than two orders of magnitude of  
 349 each other in snowpack interstitial air at Utqiagvik, AK, (Custard et al., 2017; Raso et al., 2017). Custard et al. (2017)  
 350 observed gas phase [Br<sub>2</sub>]/[Cl<sub>2</sub>] values for artificially irradiated, acidic snowpacks ranging from 2-95 for corresponding  
 351 snowpack [Br<sup>-</sup>]/[Cl<sup>-</sup>] ratios of (6 ± 1) x 10<sup>-4</sup>. Under similar conditions, Raso et al. (2017) observed [I<sub>2</sub>]/[Br<sub>2</sub>] ranging  
 352 from ~0.4-0.8 from corresponding snowpack [I<sup>-</sup>]/[Br<sup>-</sup>] amounts of (2.6±0.6) x 10<sup>-3</sup>. Despite the large differences in  
 353 relative halide abundance (i.e., [I<sup>-</sup>] << [Br<sup>-</sup>] << [Cl<sup>-</sup>]), it appears that halogen activation reaction kinetics favor the  
 354 larger halide ions, effectively levelling the relative molecular halogen production rates. The observations herein  
 355 provide an opportunity to explore the relative reactivities of OH-mediated halogen production.

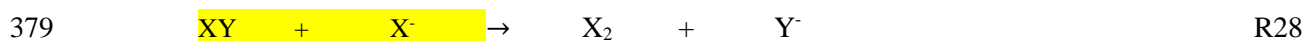
356 If we assume that the observed X<sub>2</sub> flux out of the ice is proportional to the production rate (i.e., X<sub>2</sub> desorbs  
 357 as it is produced, within the residence time of the flow tube) and that halogen production is limited by halide reaction  
 358 with OH radicals, effective relative reactivities, k<sub>X</sub><sup>-</sup>/k<sub>Y</sub><sup>-</sup>, (where X and Y represent Br, Cl, or I) can be calculated using  
 359 Eq. 1.

$$360 \frac{\text{Flux}_{X_2}}{\text{Flux}_{Y_2}} = \frac{k_{X^-}[X^-][OH][H^+]}{k_{Y^-}[Y^-][OH][H^+]} \quad (1)$$

361 The initial molecular halogen flux is calculated as the integrated sum of X<sub>2</sub> (in moles) divided by both integration time  
 362 (t = 0-3 minutes, starting from the beginning of irradiation) and the surface area of ice coverage in the flow tube.  
 363 Because the surface area, as well as the [OH] and [H<sup>+</sup>] in the ice surface reaction environment, are identical within

364 individual experiments and cancel in these calculations the relative fluxes are simply equivalent to the relative outflow  
365 concentrations of halogens. The pre-freezing halide ion concentrations (defined in Sect. 2) thus allow us to solve for  
366 the effective relative reactivity,  $k_X/k_Y$ , by assuming the ratios of the halide ice concentrations are the same after  
367 freezing.

368 At  $\text{pH} = 1.8$ ,  $k_{\text{Br}^-}/k_{\text{Cl}^-}$  was estimated to be  $(2.4 \pm 0.2) \times 10^5$  from experiment CL1; in other words, production  
369 of  $\text{Br}_2$  is 240,000 times more efficient than production of  $\text{Cl}_2$  via  $(\text{OH} + \text{halide})$  in the surface layer. Across the six  
370 experiments performed at  $\text{pH} \leq 2$  (average of 1.85) using Instant Ocean (IO3, IO4, IO5) and saltwater (SW3, SW4,  
371 SW5),  $k_{\text{I}^-}/k_{\text{Br}^-}$  was calculated to average  $(9 \pm 4) \times 10^3$  (reported uncertainty is the standard error of the mean, and thus  
372 only represents the experiment repeatability). These relative reactivities are substantially larger than the  
373 corresponding relative aqueous  $\text{OH} + \text{halide}$  rate constants ( $k_{\text{I}^-} = k_{\text{Br}^-} = 1.1 \times 10^{10} \text{ M}^{-1} \text{ s}^{-1}$  (Buxton et al., 1988; Zehavi  
374 and Rabani, 1972),  $k_{\text{Cl}^-} = 3.0 \times 10^9 \text{ M}^{-1} \text{ s}^{-1}$  (Grigor'ev et al., 1987)), which are different by less than a factor of 4.  
375 However, these rate constants refer to the specific fundamental reaction of  $\text{OH}$  with  $\text{X}^-$  to produce  $\text{HOX}$ , as in Reaction  
376 R8. Ultimately,  $\text{X}_2$  production would occur via R8-R12, and this condensed phase chemistry is much more complex  
377 when also considering interhalogen reactions, such as R28, that involve combinations of the three molecular halogens,  
378 halides, and mixed molecular halogens ( $\text{XY}$ , where  $\text{Y} = \text{Cl}, \text{Br}, \text{or I}$ ).



380 Thus, it must be that there exist competing reactions that make the production of the larger  $\text{X}_2$  more efficient. For  
381 example,  $\text{Cl} + \text{I}^- \rightarrow \text{ClI}^-$  may be faster than  $\text{Cl} + \text{Cl}^- \rightarrow \text{Cl}_2^-$ . Alternatively, the relative rates of the disproportionation  
382 reaction R11 are likely different, favoring the larger molecular halogens. We can thus only state from these  
383 observations that the apparent relative reactivities calculated are consistent with the overall reactivity of the larger  
384 ions compensating for their lower abundances. This may lead to comparable production rates in our laboratory  
385 experiments and comparable snowpack gas phase concentrations.

386 The above relative reactivity calculations are considered upper limits since the halide ratios used represent  
387 those in the pre-freezing solution. In other words, it is assumed that the ions are excluded to the ice surface reaction  
388 environment-air interface in amounts proportional to their pre-freezing concentration. Malley et al. (2018) recently  
389 demonstrated that brine can be distributed throughout ice in channels, suggesting that only the solutes at the liquid-air  
390 interface (a fraction of the total pre-freezing solution) participate in heterogeneous chemistry. Indeed, we find

391 evidence here suggesting not all ions are available for reaction at the ice brine surface, particularly for experiments  
392 for which little I<sup>-</sup> was lost from dark I<sub>2</sub> production mechanisms (i.e., pH = 4.7 with OH precursors: IO1, IO2, SW1,  
393 SW2). Considering experiment IO2 as an example (Fig. S5; pH = 4.7), integration of the I<sub>2</sub> signal during ~15 hours  
394 of exposure to both light and O<sub>3</sub> shows that 54% (82 nmol) of the original 152 nmol of I<sup>-</sup> remained unreacted in the  
395 frozen solution despite the signal apparently stabilizing at its baseline. It is therefore probable that a significant number  
396 of the ions, as well as H<sub>2</sub>O<sub>2</sub>, exist within brine channels within the ice (Bartels-Rausch et al., 2014; Malley et al.,  
397 2018). Oxidation chemistry would then be occurring throughout the ice, but release of molecular halogens to the flow  
398 tube air would be determined by diffusion rates. The diffusion rates of the product molecular halogens through bulk  
399 ice are likely slow, such that only production occurring in the brine that is in the near-liquid-air interface is observed  
400 here (Abbatt et al., 2012). Of the halogens produced from frozen solutions here, it is expected that I<sub>2</sub> is observed most  
401 readily given the high polarizability and surface affinity of I<sup>-</sup> in aqueous solutions (Gladich et al., 2011), and the  
402 relative ease of oxidation of I<sup>-</sup>. That is, surface concentrations will be relatively enhanced with larger, more polarizable  
403 anions (I<sup>-</sup> > Br<sup>-</sup> > Cl<sup>-</sup>) (Gladich et al., 2011), which favors production of I<sub>2</sub> over Br<sub>2</sub>, and Br<sub>2</sub> over Cl<sub>2</sub>. As the  
404 larger/more reactive ions are depleted through oxidation, the next largest ion then becomes more favorably oxidized.  
405 Thus, in addition to the impact of differential reactivities and competing reactions for R9-R12, what we observe in the  
406 laboratory and in the field can also be influenced by the relative surface enhancements of the anions, especially with  
407 respect to O<sub>3</sub> impacts as discussed below.

### 408 3.3 Effects of O<sub>3</sub> on halogen production

409 In experiments without an OH source (IO6-IO8, SW6-SW8), I<sub>2</sub> production was greatest when O<sub>3</sub> was  
410 introduced to the irradiated tube for both pH regimes (Table 2). The amount of I<sub>2</sub> produced over 60 minutes in these  
411 experiments was large, ranging from 26 ± 9 nmol to 80 ± 1 nmol at pH = 4.7, and from 2.6 ± 1.7 nmol to 38 ± 12 nmol  
412 at pH < 2. This production likely results from a combination of heterogeneous recycling, and the surface and aqueous  
413 reactions between O<sub>3</sub> and I<sup>-</sup> ( $k = 2.0 \times 10^{-12} \text{ cm}^3 \text{ molecules}^{-1} \text{ s}^{-1}$  (Liu et al., 2001)). While the I<sub>2</sub> produced when pH <  
414 2 appears to be lower, I<sub>2</sub> had already been produced in the presence of light prior to addition of O<sub>3</sub> (Sect. 3.2.2),  
415 yielding a lower [I<sup>-</sup>]/[Br<sup>-</sup>] ratio when O<sub>3</sub> was eventually added. Br<sub>2</sub> production amounts ranged from 0.012 ± 0.001  
416 nmol to 0.16 ± 0.01 nmol at pH = 4.7 and taking up to 6 hours to raise above detection limits after O<sub>3</sub> was added. At  
417 pH ≤ 2, Br<sub>2</sub> production amounts ranged 0.14 ± 0.02 nmol to 0.93 ± 0.05 nmol. While O<sub>3</sub>-mediated halogen production

418 has been observed directly from frozen surfaces in the absence of light in previous laboratory studies (Artiglia et al.,  
419 2017; Oldridge and Abbatt, 2011; Oum et al., 1998a; Wren et al., 2013), Br<sub>2</sub> production has not been directly observed  
420 from the Arctic snowpack without irradiation (Pratt et al., 2013). This raises a question of the role of O<sub>3</sub> in initial  
421 halogen release in the Arctic spring.

422 When OH-precursors were present, the addition of O<sub>3</sub> to the zero-air flow over the irradiated frozen sample  
423 caused additional production of I<sub>2</sub> and Br<sub>2</sub>, as shown in Figure 2a and b, under both pH regimes (Table 2). In  
424 experiments at pH ≈ 4.7 in which [I<sup>-</sup>]/[Br<sup>-</sup>] remained sufficiently large due to minimal dark production of I<sub>2</sub> (i.e., IO1-  
425 2, SW1-2), exposure to O<sub>3</sub> caused a sharp increase in I<sub>2</sub> (as in Fig. 2a). I<sub>2</sub> production amounts for frozen Instant Ocean  
426 at pH ≈ 4.7 (IO1, IO2) averaged 22 ± 10 nmol, about two times less than for frozen saltwater experiments SW1 and  
427 SW2 (average production amount of 51 ± 25 nmol). As the I<sub>2</sub> signal decayed, the corresponding Br<sub>2</sub> signals gradually  
428 increased above detection limits, approximately 3h after the introduction of O<sub>3</sub> (Fig. 2a). The average integrated  
429 amounts of Br<sub>2</sub> produced from these pH ≈ 4.7 experiments were very similar (0.05 ± 0.01 nmol for IO experiments  
430 and 0.03 ± 0.01 nmol for SW experiments).

431 When pH < 2, the effects of O<sub>3</sub> addition varied according to the remaining availability of I<sup>-</sup>. When the surface  
432 I<sup>-</sup> reservoir had been reduced from dark reactions with H<sub>2</sub>O<sub>2</sub> or NO<sub>2</sub><sup>-</sup> (R17-21; Sect. 3.1), exposure to O<sub>3</sub> did not  
433 increase I<sub>2</sub> above the LOD except in experiment IO5, which exhibited a small spike before decaying below the LOD  
434 (0.11 ± 0.06 nmol in IO5). However, O<sub>3</sub> did cause additional Br<sub>2</sub> production after one hour (average of 10 ± 2 nmol  
435 for IO4 (Fig. 2b) and IO5 (Fig S4), and 14 ± 2 nmol for SW4 and SW5). In contrast, for SW3 (using NO<sub>2</sub><sup>-</sup> as an OH  
436 source), there was relatively little initial consumption of I<sup>-</sup> by dark reaction; therefore, when O<sub>3</sub> was added, 1.1 ± 0.1  
437 nmol additional I<sub>2</sub> was observed, comparable to what was observed with the higher pH experiments (Fig. S5). The  
438 amount of Br<sub>2</sub> produced (0.46 ± 0.01 nmol) was also significantly less than observed when I<sup>-</sup> was initially depleted,  
439 demonstrating the importance of the halide ratios.

440 This additional O<sub>3</sub>-induced halogen production could result from a combination of mechanisms. First, as  
441 discussed above, O<sub>3</sub> can react with halides on frozen saline surfaces to produce Br<sub>2</sub> or I<sub>2</sub> per reactions R18-19, and  
442 then R4 (Artiglia et al., 2017; Carpenter et al., 2013; Gladich et al., 2015; Hayase et al., 2010; Oum et al., 1998a;  
443 Shaw and Carpenter, 2013; Wren et al., 2013). It is possible that Br<sub>2</sub> (as well as other halogens) may have been  
444 produced via this mechanism at levels below the LOD in previous Arctic snowpack studies (Custard et al., 2017; Pratt  
445 et al., 2013; Raso et al., 2017).

446 The presence of O<sub>3</sub> also yielded HOX compounds (Fig. 3-4), likely formed in the flowtube in part by O<sub>3</sub>  
447 reactions with halides (R18-R19). Additionally, given a flow tube residence time of 12 seconds, gas phase production  
448 of HOX is possible via R1-R3 and could act as an additional X<sub>2</sub> production source (via R4), given a timescale for  
449 molecular diffusion of 6.5 seconds for HOBr from the center of the tube to the ice surface. At this flow rate, there is  
450 enough time for 1-2 heterogeneous reaction cycles. Figure 3 shows HOX for IO<sub>2</sub> (pH=4.7 with H<sub>2</sub>O<sub>2</sub> present,  
451 analogous to IO<sub>1</sub>, SW1, SW2). For each experiment in this series, increases in I<sub>2</sub>, HOI, and Br<sub>2</sub> were readily observed  
452 when the O<sub>3</sub> was introduced at hour 2 (Fig. 3, Fig. S4). However, corresponding HOBr production was not observed,  
453 perhaps either due to a high LOD, or the relatively low abundance of Br<sub>2</sub> that would limit production of HOBr.  
454 Conversely, in pH ≤ 2 cases when substantial portions of I<sup>-</sup> had already reacted prior to irradiation (IO<sub>4</sub>, IO<sub>5</sub>, SW<sub>4</sub>,  
455 SW<sub>5</sub>), the addition of O<sub>3</sub> produced negligible amounts of I<sub>2</sub> and HOI (Fig. 4). But, in these cases, following the  
456 addition of O<sub>3</sub>, HOBr (*m/z* 225 IHO<sup>81</sup>Br<sup>-</sup>), was observed together with Br<sub>2</sub> (Fig. 4, Fig. S4). We note in this case that  
457 *m/z* 223, representative of IHO<sup>79</sup>Br<sup>-</sup>, does not appear to show an enhancement when O<sub>3</sub> is added to the system. There  
458 was a much higher background signal for *m/z* 223 compared with *m/z* 225 (IHO<sup>81</sup>Br<sup>-</sup>) resulting from an unknown  
459 interference.

#### 460 4 Summary and Conclusions

461 It was shown in this ice-coated wall flow tube laboratory study that the hydroxyl radical can act as an effective  
462 condensed-phase halide oxidant leading to I<sub>2</sub>, IBr, Br<sub>2</sub>, and Cl<sub>2</sub> production under acidic conditions. Rates of molecular  
463 halogen production and release were dictated by both pH and relative halide concentrations. The identities of the  
464 molecular halogens produced appears to be highly influenced by which ions are enhanced at the ice surface, with I<sub>2</sub>  
465 production occurring prior to Br<sub>2</sub> production, which commenced as the [I<sup>-</sup>]/[Br<sup>-</sup>] was reduced. An opportunity exists  
466 to further explore this chemistry via surface-sensitive methods, for which recent developments have been shown to  
467 effectively enable characterization of the surface composition of frozen solutions of sodium chloride under near  
468 atmospherically relevant conditions (Artiglia et al., 2017; Orlando et al., 2016). It would be useful to confirm the  
469 dominant ions involved in this surface-based chemistry over time. Further investigations into the effects of halide  
470 ratios on halogen production are also suggested, including measurements of how the ratios vary for different frozen  
471 Arctic surfaces, as well as how they vary spatially. While condensed-phase OH produces Br<sub>2</sub> and I<sub>2</sub> most rapidly in

472 this study, it appears that other mechanisms, such as heterogeneous recycling of HOCl or ClONO<sub>2</sub>, could be a more  
473 dominant mechanism for in situ production of gas phase Cl<sub>2</sub> (Wang and Pratt, 2017). We find the addition of gas phase  
474 O<sub>3</sub> produces additional Br<sub>2</sub> and I<sub>2</sub>, likely through aqueous reactions with halides and/or gas-phase production of HOX  
475 or possibly XONO<sub>2</sub> (Deiber et al., 2004) and subsequent halogen explosion chemistry. These results lend support for  
476 the photochemical, condensed-phase molecular halogen production mechanisms proposed by the recent in situ  
477 snowpack experiments (Custard et al., 2017; Pratt et al., 2013; Raso et al., 2017).

478         Understanding the environmental pH-dependence of halogen activation necessitates study of the pH on  
479 relevant Arctic frozen surfaces. Pratt et al. (2013) found that the frozen surfaces most conducive to in-situ  
480 photochemical Br<sub>2</sub> production had acidic pH after melting, while no production was observed from those with a well-  
481 buffered alkaline ice brine. Similarly, we find herein that condensed-phase OH-induced halogen production is  
482 enhanced at lower pH. Wren and Donaldson (2012a, 2012b) found in laboratory studies that pH of acidic and basic  
483 solutions remains essentially unchanged after freezing, and that saline solutions with buffers (i.e., seawater) maintain  
484 their buffering capacity following trace gas deposition, supporting the lack of observed Br<sub>2</sub> production from the sea  
485 ice surface (Pratt et al., 2013). Therefore, it would be useful to test in-situ production of halogens from Arctic frozen  
486 surfaces in tandem with measurement of the pH of said surfaces to determine the atmospherically relevant surface pH  
487 range required for halogen production.

488  
489 *Data availability.* Halfacre, J. W., Shepson, P. B., Pratt, K. A.: Laboratory experiments of the pH-dependent  
490 production of molecular chlorine, bromine, and iodine from frozen saline surfaces, NSF Arctic Data Center,  
491 <http://dx.doi.org/10.18739/A22804Z17>, 2018

492  
493 *Author contributions.* JWH and PBS designed the research and JWH performed the experiments and data  
494 analysis. All three authors contributed to the discussion and interpretation of the results and writing of the paper.

495  
496 *Competing interests.* The authors declare that they have no conflict of interest.

497 **Acknowledgements**

498 We thank the National Science Foundation for their funding (PLR-1417668 and PLR-1417906, OPP-1417668).  
499 We also express thanks to J. H. Slade, L. G. Huey, D. J. Tanner, F. Xiong, A. R. W. Raso, and K. D. Custard for their  
500 assistance with CIMS operation and maintenance. Additionally, we thank the Purdue Chemistry Shop for helping  
501 build both the cooling and photolysis boxes, as well as the Jonathan Amy Facility for Chemical Instrumentation for  
502 their support in the fabrication of the experimental flow tube and setup of our experimental boxes. Thanks are also  
503 extended to M. Haas and M. Bischoff for performing total organic carbon analysis of our samples, and A. R. W. Raso  
504 for confirmation of the iodide concentrations in our Instant Ocean samples. Finally, we thank T. Miller and the Purdue  
505 Birck Nanotechnology Center for the provision of the nano-grade water used for our samples.

506 **References**

507 Abbatt, J., Oldridge, N., Symington, A., Chukalovskiy, V., McWhinney, R. D., Sjostedt, S. and Cox, R. A.: Release  
508 of Gas-Phase Halogens by Photolytic Generation of OH in Frozen Halide–Nitrate Solutions: An Active Halogen  
509 Formation Mechanism?, *J. Phys. Chem. A*, 114(23), 6527–6533, doi:10.1021/jp102072t, 2010.

510 Abbatt, J. P. D., Thomas, J. L., Abrahamsson, K., Boxe, C., Granfors, A., Jones, A. E., King, M. D., Saiz-Lopez, A.,  
511 Shepson, P. B., Sodeau, J., Toohey, D. W., Toubin, C., von Glasow, R., Wren, S. N. and Yang, X.: Halogen activation  
512 via interactions with environmental ice and snow in the polar lower troposphere and other regions, *Atmos Chem Phys*,  
513 12(14), 6237–6271, doi:10.5194/acp-12-6237-2012, 2012.

514 Artiglia, L., Edebeli, J., Orlando, F., Chen, S., Lee, M.-T., Corral Arroyo, P., Gilgen, A., Bartels-Rausch, T., Kleibert,  
515 A., Vazdar, M., Andres Carignano, M., Francisco, J. S., Shepson, P. B., Gladich, I. and Ammann, M.: A surface-  
516 stabilized ozonide triggers bromide oxidation at the aqueous solution-vapour interface, *Nat. Commun.*, 8(1),  
517 doi:10.1038/s41467-017-00823-x, 2017.

518 Barrie, L. and Platt, U.: Arctic tropospheric chemistry: an overview, *Tellus B*, 49(5), 450–454, doi:10.1034/j.1600-  
519 0889.49.issue5.2.x, 1997.

520 Bartels-Rausch, T., Jacobi, H.-W., Kahan, T. F., Thomas, J. L., Thomson, E. S., Abbatt, J. P. D., Ammann, M.,  
521 Blackford, J. R., Bluhm, H., Boxe, C., Domine, F., Frey, M. M., Gladich, I., Guzmán, M. I., Heger, D., Huthwelker,  
522 T., Klán, P., Kuhs, W. F., Kuo, M. H., Maus, S., Moussa, S. G., McNeill, V. F., Newberg, J. T., Pettersson, J. B. C.,

523 Roeselová, M. and Sodeau, J. R.: A review of air–ice chemical and physical interactions (AICI): liquids, quasi-liquids,  
524 and solids in snow, *Atmos Chem Phys*, 14(3), 1587–1633, doi:10.5194/acp-14-1587-2014, 2014.

525 Buxton, G. V., Greenstock, C. L., Helman, W. P. and Ross, A. B.: Critical Review of rate constants for reactions of  
526 hydrated electrons, hydrogen atoms and hydroxyl radicals ( $\cdot\text{OH}/\cdot\text{O}^-$  in Aqueous Solution, *J. Phys. Chem. Ref. Data*,  
527 17(2), 513–886, doi:10.1063/1.555805, 1988.

528 Carpenter, L. J., MacDonald, S. M., Shaw, M. D., Kumar, R., Saunders, R. W., Parthipan, R., Wilson, J. and Plane, J.  
529 M. C.: Atmospheric iodine levels influenced by sea surface emissions of inorganic iodine, *Nat. Geosci.*, 6(2), 108–  
530 111, doi:10.1038/ngeo1687, 2013.

531 Cho, H., Shepson, P. B., Barrie, L. A., Cowin, J. P. and Zaveri, R.: NMR Investigation of the Quasi-Brine Layer in  
532 Ice/Brine Mixtures, *J. Phys. Chem. B*, 106(43), 11226–11232, doi:10.1021/jp020449+, 2002.

533 Custard, K. D., Pratt, K. A., Wang, S. and Shepson, P. B.: Constraints on Arctic Atmospheric Chlorine Production  
534 through Measurements and Simulations of  $\text{Cl}_2$  and  $\text{ClO}$ , *Environ. Sci. Technol.*, 50(22), 12394–12400,  
535 doi:10.1021/acs.est.6b03909, 2016.

536 Custard, K. D., Raso, A. R. W., Shepson, P. B., Staebler, R. M. and Pratt, K. A.: Production and Release of Molecular  
537 Bromine and Chlorine from the Arctic Coastal Snowpack, *ACS Earth Space Chem.*, 1(3), 142–151,  
538 doi:10.1021/acsearthspacechem.7b00014, 2017.

539 Deiber, G., George, C., Calvé, S. L., Schweitzer, F. and Mirabel, P.: Uptake study of  $\text{ClONO}_2$  and  $\text{BrONO}_2$  by Halide  
540 containing droplets, *Atmospheric Chem. Phys.*, 4(5), 1291–1299, doi:https://doi.org/10.5194/acp-4-1291-2004, 2004.

541 Fickert, S., Adams, J. W. and Crowley, J. N.: Activation of  $\text{Br}_2$  and  $\text{BrCl}$  via uptake of  $\text{HOBr}$  onto aqueous salt  
542 solutions, *J. Geophys. Res. Atmospheres*, 104(D19), 23719–23727, doi:10.1029/1999JD900359, 1999.

543 France, J. L., Reay, H. J., King, M. D., Voisin, D., Jacobi, H. W., Domine, F., Beine, H., Anastasio, C., MacArthur,  
544 A. and Lee-Taylor, J.: Hydroxyl radical and  $\text{NO}_x$  production rates, black carbon concentrations and light-absorbing  
545 impurities in snow from field measurements of light penetration and nadir reflectivity of onshore and offshore coastal  
546 Alaskan snow, *J. Geophys. Res.*, 117, doi:10.1029/2011JD016639, 2012.

547 Garland, J. A. and Curtis, H.: Emission of iodine from the sea surface in the presence of ozone, *J. Geophys. Res.*,  
548 86(C4), 3183, doi:10.1029/JC086iC04p03183, 1981.

549 Gladich, I., Shepson, P. B., Carignano, M. A. and Szleifer, I.: Halide Affinity for the Water–Air Interface in Aqueous  
550 Solutions of Mixtures of Sodium Salts, *J. Phys. Chem. A*, 115(23), 5895–5899, doi:10.1021/jp110208a, 2011.

551 Gladich, I., Francisco, J. S., Buszek, R. J., Vazdar, M., Carignano, M. A. and Shepson, P. B.: Ab Initio Study of the  
552 Reaction of Ozone with Bromide Ion, *J. Phys. Chem. A*, 119(19), 4482–4488, doi:10.1021/jp5101279, 2015.

553 Grigor'ev, A. E., Makarov, I. E. and Pikaev, A. K.: Formation of  $\text{Cl}_2^-$  in the bulk of solution during radiolysis of  
554 concentrated aqueous solutions of chlorides, *Khimiya Vysok. Ehnergij*, 21(2), 123–126, 1987.

555 Hayase, S., Yabushita, A., Kawasaki, M., Enami, S., Hoffmann, M. R. and Colussi, A. J.: Heterogeneous Reaction of  
556 Gaseous Ozone with Aqueous Iodide in the Presence of Aqueous Organic Species, *J. Phys. Chem. A*, 114(19), 6016–  
557 6021, doi:10.1021/jp101985f, 2010.

558 Hellebust, S., Roddis, T. and Sodeau, J. R.: Potential Role of the Nitroacidium Ion on HONO Emissions from the  
559 Snowpack, *J. Phys. Chem. A*, 111(7), 1167–1171, doi:10.1021/jp068264g, 2007.

560 Herring, J. R. and Liss, P. S.: A new method for the determination of iodine species in seawater, *Deep Sea Res.*  
561 *Oceanogr. Abstr.*, 21(9), 777–783, doi:10.1016/0011-7471(74)90085-0, 1974.

562 Kim, K., Yabushita, A., Okumura, M., Saiz-Lopez, A., Cuevas, C. A., Blaszcak-Boxe, C. S., Min, D. W., Yoon, H.-  
563 I. and Choi, W.: Production of Molecular Iodine and Tri-iodide in the Frozen Solution of Iodide: Implication for Polar  
564 Atmosphere, *Environ. Sci. Technol.*, 50(3), 1280–1287, doi:10.1021/acs.est.5b05148, 2016.

565 Knipping, E. M., Lakin, M. J., Foster, K. L., Jungwirth, P., Tobias, D. J., Gerber, R. B., Dabdub, D. and Finlayson-  
566 Pitts, B. J.: Experiments and Simulations of Ion-Enhanced Interfacial Chemistry on Aqueous NaCl Aerosols, *Science*,  
567 288(5464), 301–306, doi:10.1126/science.288.5464.301, 2000.

568 Küpper, F. C., Schweigert, N., Gall, E. A., Legendre, J.-M., Vilter, H. and Kloareg, B.: Iodine uptake in Laminariales  
569 involves extracellular, haloperoxidase-mediated oxidation of iodide, *Planta*, 207(2), 163–171,  
570 doi:10.1007/s004250050469, 1998.

571 Liao, J., Huey, L. G., Tanner, D. J., Flocke, F. M., Orlando, J. J., Neuman, J. A., Nowak, J. B., Weinheimer, A. J.,  
572 Hall, S. R., Smith, J. N., Fried, A., Staebler, R. M., Wang, Y., Koo, J.-H., Cantrell, C. A., Weibring, P., Walega, J.,  
573 Knapp, D. J., Shepson, P. B. and Stephens, C. R.: Observations of inorganic bromine (HOBr, BrO, and  $\text{Br}_2$ ) speciation  
574 at Barrow, Alaska, in spring 2009, *J. Geophys. Res. Atmospheres*, 117(D14), D00R16, doi:10.1029/2011JD016641,  
575 2012.

576 Liao, J., Huey, L. G., Liu, Z., Tanner, D. J., Cantrell, C. A., Orlando, J. J., Flocke, F. M., Shepson, P. B., Weinheimer,  
577 A. J., Hall, S. R., Ullmann, K., Beine, H. J., Wang, Y., Ingall, E. D., Stephens, C. R., Hornbrook, R. S., Apel, E. C.,

578 Riemer, D., Fried, A., Mauldin Iii, R. L., Smith, J. N., Staebler, R. M., Neuman, J. A. and Nowak, J. B.: High levels  
579 of molecular chlorine in the Arctic atmosphere, *Nat. Geosci.*, 7(2), 91–94, doi:10.1038/ngeo2046, 2014.

580 Liu, Q., Schurter, L. M., Muller, C. E., Aloisio, S., Francisco, J. S. and Margerum, D. W.: Kinetics and Mechanisms  
581 of Aqueous Ozone Reactions with Bromide, Sulfite, Hydrogen Sulfite, Iodide, and Nitrite Ions, *Inorg. Chem.*, 40(17),  
582 4436–4442, doi:10.1021/ic000919j, 2001.

583 Lockwood, A. L., Shepson, P. B., Fiddler, M. N. and Alaghmand, M.: Isoprene nitrates: preparation, separation,  
584 identification, yields, and atmospheric chemistry, *Atmos Chem Phys*, 10(13), 6169–6178, doi:10.5194/acp-10-6169-  
585 2010, 2010.

586 Luther, G. W., Swartz, C. B. and Ullman, W. J.: Direct determination of iodide in seawater by cathodic stripping  
587 square wave voltammetry, *Anal. Chem.*, 60(17), 1721–1724, doi:10.1021/ac00168a017, 1988.

588 Malley, P. P. A., Chakraborty, S. and Kahan, T. F.: Physical Characterization of Frozen Saltwater Solutions Using  
589 Raman Microscopy, *ACS Earth Space Chem.*, doi:10.1021/acsearthspacechem.8b00045, 2018.

590 McConnell, J. C., Henderson, G. S., Barrie, L., Bottenheim, J., Niki, H., Langford, C. H. and Templeton, E. M. J.:  
591 Photochemical bromine production implicated in Arctic boundary-layer ozone depletion, *Nature*, 355(6356), 150–  
592 152, doi:10.1038/355150a0, 1992.

593 Neuman, J. A., Nowak, J. B., Huey, L. G., Burkholder, J. B., Dibb, J. E., Holloway, J. S., Liao, J., Peischl, J., Roberts,  
594 J. M., Ryerson, T. B., Scheuer, E., Stark, H., Stickel, R. E., Tanner, D. J. and Weinheimer, A.: Bromine measurements  
595 in ozone depleted air over the Arctic Ocean, *Atmos Chem Phys*, 10(14), 6503–6514, doi:10.5194/acp-10-6503-2010,  
596 2010.

597 O’Driscoll, P., Lang, K., Minogue, N. and Sodeau, J.: Freezing Halide Ion Solutions and the Release of Interhalogens  
598 to the Atmosphere, *J. Phys. Chem. A*, 110(14), 4615–4618, doi:10.1021/jp060491v, 2006.

599 O’Driscoll, P., Minogue, N., Takenaka, N. and Sodeau, J.: Release of Nitric Oxide and Iodine to the Atmosphere from  
600 the Freezing of Sea-Salt Aerosol Components, *J. Phys. Chem. A*, 112(8), 1677–1682, doi:10.1021/jp710464c, 2008.

601 Oldridge, N. W. and Abbatt, J. P. D.: Formation of Gas-Phase Bromine from Interaction of Ozone with Frozen and  
602 Liquid NaCl/NaBr Solutions: Quantitative Separation of Surficial Chemistry from Bulk-Phase Reaction, *J. Phys.*  
603 *Chem. A*, 115(12), 2590–2598, doi:10.1021/jp200074u, 2011.

604 Orlando, F., Waldner, A., Bartels-Rausch, T., Birrer, M., Kato, S., Lee, M.-T., Proff, C., Huthwelker, T., Kleibert, A.,  
605 Bokhoven, J. van and Ammann, M.: The Environmental Photochemistry of Oxide Surfaces and the Nature of Frozen  
606 Salt Solutions: A New in Situ XPS Approach, *Top. Catal.*, 1–14, doi:10.1007/s11244-015-0515-5, 2016.

607 O’Sullivan, D. and Sodeau, J. R.: Freeze-Induced Reactions: Formation of Iodine–Bromine Interhalogen Species from  
608 Aqueous Halide Ion Solutions, *J. Phys. Chem. A*, 114(46), 12208–12215, doi:10.1021/jp104910p, 2010.

609 Oum, K. W., Lakin, M. J. and Finlayson-Pitts, B. J.: Bromine activation in the troposphere by the dark reaction of O<sub>3</sub>  
610 with seawater ice, *Geophys. Res. Lett.*, 25(21), 3923–3926, doi:10.1029/1998GL900078, 1998a.

611 Oum, K. W., Lakin, M. J., DeHaan, D. O., Brauers, T. and Finlayson-Pitts, B. J.: Formation of Molecular Chlorine  
612 from the Photolysis of Ozone and Aqueous Sea-Salt Particles, *Science*, 279(5347), 74–76,  
613 doi:10.1126/science.279.5347.74, 1998b.

614 Platt, U. and Hönninger, G.: The role of halogen species in the troposphere, *Chemosphere*, 52(2), 325–338,  
615 doi:10.1016/S0045-6535(03)00216-9, 2003.

616 Pratt, K. A., Custard, K. D., Shepson, P. B., Douglas, T. A., Pöhler, D., General, S., Zielcke, J., Simpson, W. R., Platt,  
617 U., Tanner, D. J., Gregory Huey, L., Carlsen, M. and Stirm, B. H.: Photochemical production of molecular bromine  
618 in Arctic surface snowpacks, *Nat. Geosci.*, 6(5), 351–356, doi:10.1038/ngeo1779, 2013.

619 Raso, A. R. W., Custard, K. D., May, N. W., Tanner, D., Newburn, M. K., Walker, L., Moore, R. J., Huey, L. G.,  
620 Alexander, L., Shepson, P. B. and Pratt, K. A.: Active molecular iodine photochemistry in the Arctic, *Proc. Natl.*  
621 *Acad. Sci.*, 114(38), 10053–10058, doi:10.1073/pnas.1702803114, 2017.

622 Saiz-Lopez, A. and von Glasow, R.: Reactive halogen chemistry in the troposphere, *Chem. Soc. Rev.*, 41(19), 6448–  
623 6472, doi:10.1039/C2CS35208G, 2012.

624 Shaw, M. D. and Carpenter, L. J.: Modification of Ozone Deposition and I<sub>2</sub> Emissions at the Air–Aqueous Interface  
625 by Dissolved Organic Carbon of Marine Origin, *Environ. Sci. Technol.*, 47(19), 10947–10954,  
626 doi:10.1021/es4011459, 2013.

627 Simpson, W. R., von Glasow, R., Riedel, K., Anderson, P., Ariya, P., Bottenheim, J., Burrows, J., Carpenter, L. J.,  
628 Frieß, U., Goodsite, M. E., Heard, D., Hutterli, M., Jacobi, H.-W., Kaleschke, L., Neff, B., Plane, J., Platt, U., Richter,  
629 A., Roscoe, H., Sander, R., Shepson, P., Sodeau, J., Steffen, A., Wagner, T. and Wolff, E.: Halogens and their role in  
630 polar boundary-layer ozone depletion, *Atmos Chem Phys*, 7(16), 4375–4418, doi:10.5194/acp-7-4375-2007, 2007.

631 Simpson, W. R., Brown, S. S., Saiz-Lopez, A., Thornton, J. A. and Glasow, R. von: Tropospheric Halogen Chemistry:  
632 Sources, Cycling, and Impacts, *Chem. Rev.*, 115(10), 4035–4062, doi:10.1021/cr5006638, 2015.

633 Sjostedt, S. J. and Abbatt, J. P. D.: Release of gas-phase halogens from sodium halide substrates: heterogeneous  
634 oxidation of frozen solutions and desiccated salts by hydroxyl radicals, *Environ. Res. Lett.*, 3(4), 045007,  
635 doi:10.1088/1748-9326/3/4/045007, 2008.

636 Steffen, A., Douglas, T., Amyot, M., Ariya, P., Aspmo, K., Berg, T., Bottenheim, J., Brooks, S., Cobbett, F., Dastoor,  
637 A., Dommergue, A., Ebinghaus, R., Ferrari, C., Gardfeldt, K., Goodsite, M. E., Lean, D., Poulain, A. J., Scherz, C.,  
638 Skov, H., Sommar, J. and Temme, C.: A synthesis of atmospheric mercury depletion event chemistry in the  
639 atmosphere and snow, *Atmospheric Chem. Phys.*, 8(6), 1445–1482, doi:10.5194/acp-8-1445-2008, 2008.

640 Steffen, A., Bottenheim, J., Cole, A., Ebinghaus, R., Lawson, G. and Leitch, W. R.: Atmospheric mercury speciation  
641 and mercury in snow over time at Alert, Canada, *Atmos Chem Phys*, 14(5), 2219–2231, doi:10.5194/acp-14-2219-  
642 2014, 2014.

643 Tang, T. and McConnell, J. C.: Autocatalytic release of bromine from Arctic snow pack during polar sunrise, *Geophys.*  
644 *Res. Lett.*, 23(19), 2633–2636, doi:10.1029/96GL02572, 1996.

645 Tsunogai, S. and Sase, T.: Formation of iodide-iodine in the ocean, *Deep Sea Res. Oceanogr. Abstr.*, 16(5), 489–496,  
646 doi:10.1016/0011-7471(69)90037-0, 1969.

647 Vogt, R., Crutzen, P. J. and Sander, R.: A mechanism for halogen release from sea-salt aerosol in the remote marine  
648 boundary layer, *Nature*, 383(6598), 327–330, doi:10.1038/383327a0, 1996.

649 Wang, S. and Pratt, K. A.: Molecular Halogens above the Arctic Snowpack: Emissions, Diurnal Variations, and  
650 Recycling Mechanisms, *J. Geophys. Res. Atmospheres*, 2017.

651 Weaver, J. R.: Birck Nanotechnology Center Technical Overview, edited by Purdue University Office of Research  
652 and Partnerships, [online] Available from: <http://docs.lib.purdue.edu/gendes/5> (Accessed 28 January 2016), 2015.

653 Wennberg, P.: Atmospheric chemistry: Bromine explosion, *Nature*, 397(6717), 299–301, doi:10.1038/16805, 1999.

654 Wren, S. N. and Donaldson, D. J.: How does deposition of gas phase species affect pH at frozen salty interfaces?,  
655 *Atmospheric Chem. Phys.*, 12(21), 10065–10073, doi:<https://doi.org/10.5194/acp-12-10065-2012>, 2012a.

656 Wren, S. N. and Donaldson, D. J.: Laboratory Study of pH at the Air–Ice Interface, *J. Phys. Chem. C*, 116(18), 10171–  
657 10180, doi:10.1021/jp3021936, 2012b.

658 Wren, S. N., Donaldson, D. J. and Abbatt, J. P. D.: Photochemical chlorine and bromine activation from artificial  
659 saline snow, *Atmos Chem Phys*, 13(19), 9789–9800, doi:10.5194/acp-13-9789-2013, 2013.

660 Xiong, F., McAvey, K. M., Pratt, K. A., Groff, C. J., Hostetler, M. A., Lipton, M. A., Starn, T. K., Seeley, J. V.,  
661 Bertman, S. B., Teng, A. P., Crouse, J. D., Nguyen, T. B., Wennberg, P. O., Misztal, P. K., Goldstein, A. H.,  
662 Guenther, A. B., Koss, A. R., Olson, K. F., de Gouw, J. A., Baumann, K., Edgerton, E. S., Feiner, P. A., Zhang, L.,  
663 Miller, D. O., Brune, W. H. and Shepson, P. B.: Observation of isoprene hydroxynitrates in the southeastern United  
664 States and implications for the fate of NO<sub>x</sub>, *Atmos Chem Phys*, 15(19), 11257–11272, doi:10.5194/acp-15-11257-  
665 2015, 2015.

666 Zehavi, D. and Rabani, J.: Oxidation of aqueous bromide ions by hydroxyl radicals. Pulse radiolytic investigation, *J.*  
667 *Phys. Chem.*, 76(3), 312–319, doi:10.1021/j100647a006, 1972.

668

669 **Tables**

670 Table 1: List of relevant species monitored by chemical ionization mass spectrometry ( $\text{I}(\text{H}_2\text{O})_n^-$  as reagent ion) with corresponding  
 671  $m/z$  values.

Species	$m/z$
$\text{I}^{81}\text{Br}^-$	208
$\text{I}^{79}\text{Br}^{79}\text{Br}^-$	285
$\text{I}^{79}\text{Br}^{81}\text{Br}^-$	287
$\text{I}^{35}\text{Cl}^-$	162
$\text{I}^{37}\text{Cl}^-$	164
$\text{I}^{35}\text{Cl}^{35}\text{Cl}^-$	197
$\text{I}^{35}\text{Cl}^{37}\text{Cl}^-$	199
$\text{I}^{37}\text{Cl}^{37}\text{Cl}^-$	201
$\text{I}^{79}\text{Br}^{35}\text{Cl}^-$	241
$\text{I}^{81}\text{Br}^{35}\text{Cl}^- / \text{I}^{79}\text{Br}^{37}\text{Cl}^-$	243
$\text{I}_3^-$	381
$\text{IHO}^{79}\text{Br}$	223
$\text{IHO}^{81}\text{Br}$	225
$\text{IHO}_3^{5}\text{Cl}^-$	179
$\text{IHO}_3^{7}\text{Cl}^-$	181
$\text{IHOI}^-$	271
$\text{I}^{79}\text{IBr}^-$	333
$\text{I}^{81}\text{IBr}^-$	335

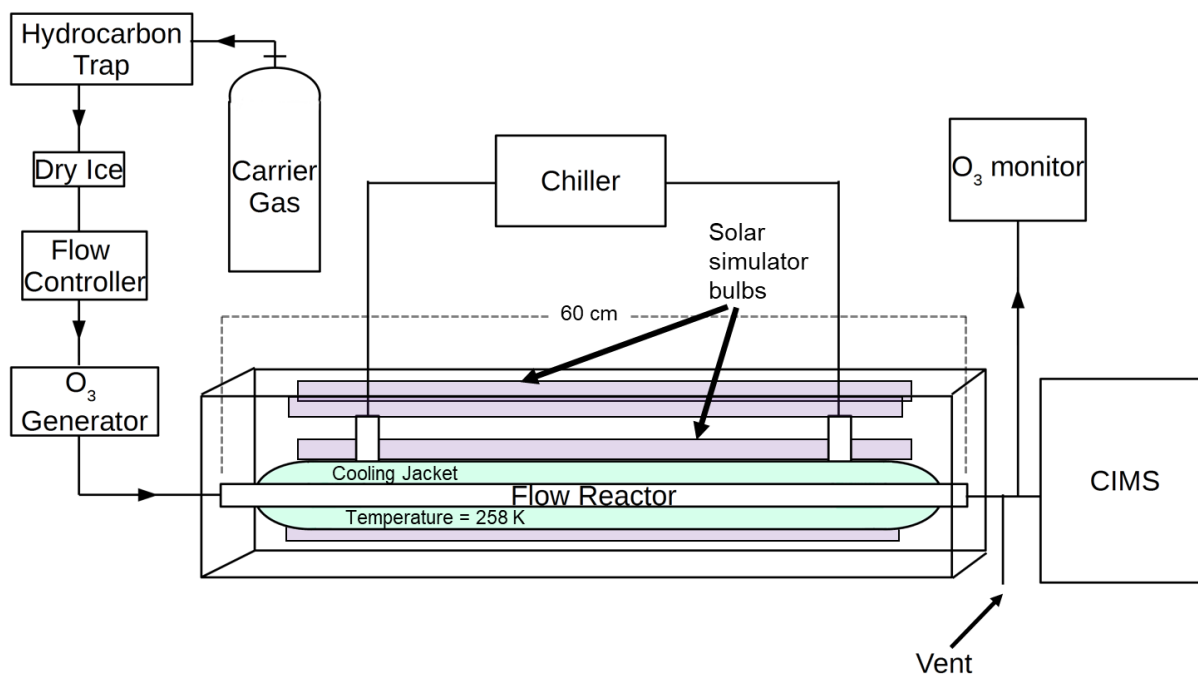
672

673

674 Table 2: Results for all experiments performed. The first line in an experiment represents the integrated totals of molecular halogen  
 675 production after 1 hour of irradiation (t = 0 through t = 1 h). The results on italicized lines are 1 h integrated production amounts  
 676 beginning once additional ozone was introduced to the flow tube. Average LODs across experiments were  $1.8 \pm 0.4$ ,  $1.2 \pm 0.3$ ,  
 677 and  $9 \pm 2$  pmol mol<sup>-1</sup> for Br<sub>2</sub>, Cl<sub>2</sub>, and I<sub>2</sub> respectively. "IO#" represents samples composed of Instant Ocean, and "SW#" represents  
 678 "saltwater" samples, composed of reagent salts. "CL1" here represents the experiment performed using 0.557M high purity NaCl.  
 679 \*The Br<sub>2</sub> and I<sub>2</sub> values presented for IO2 are discussed further in the Supplemental Information.

Experiment	Oxidant	pH	I <sub>2</sub> produced (nmol)	Br <sub>2</sub> produced (nmol)	Cl <sub>2</sub> produced (nmol)
IO1	H <sub>2</sub> O <sub>2</sub> +O <sub>3</sub>	4.7	9 (±3) 22 (±8)	< LOD <i>0.06 (±0.05)</i>	
IO2	H <sub>2</sub> O <sub>2</sub> +O <sub>3</sub>	4.7	*0.6 (±0.4) <i>21 (±14)</i>	*0.034 (±0.003) <i>0.038 (±0.003)</i>	
SW1	H <sub>2</sub> O <sub>2</sub> +O <sub>3</sub>	4.7	6.0 (±2.1) <i>51 (±19)</i>	< LOD <i>0.024(±0.014)</i>	
SW2	H <sub>2</sub> O <sub>2</sub> +O <sub>3</sub>	4.5	8 (±4) <i>51 (±25)</i>	< LOD <i>0.018 (±0.003)</i>	
IO3	NO <sub>2</sub> <sup>-</sup>	2.0	39 (±1)	0.084 (±0.002)	
IO4	H <sub>2</sub> O <sub>2</sub> +O <sub>3</sub>	1.7	0.8 (±0.3) < LOD	5.6 (±0.3) <i>12 (±1)</i>	
IO5	H <sub>2</sub> O <sub>2</sub> +O <sub>3</sub>	1.7	0.33 (±0.11) <i>0.11 (±0.04)</i>	3.5 (±0.4) <i>9.2 (±1.0)</i>	
SW3	NO <sub>2</sub> <sup>-</sup> +O <sub>3</sub>	1.8	4.0 (±0.1) < LOD	< LOD <i>0.46 (±0.1)</i>	
SW4	NO <sub>2</sub> <sup>-</sup> +O <sub>3</sub>	2.2	< LOD < LOD	5.4 (±0.7) <i>13 (±2)</i>	
SW5	H <sub>2</sub> O <sub>2</sub> +O <sub>3</sub>	1.8	0.75 (±0.26) < LOD	6.0 (±0.7) <i>15 (±2)</i>	
CL1	H <sub>2</sub> O <sub>2</sub>	1.8	0.10 (±0.03)	0.10 (±0.01)	0.093 (±0.008)
IO6	None +O <sub>3</sub>	4.7	< LOD 26 (±9)	< LOD <i>0.015 (±0.001)</i>	
IO7	None +O <sub>3</sub>	4.7	0.10 (±0.06) <i>47 (±29)</i>	< LOD <i>0.012 (±0.001)</i>	
SW6	None +O <sub>3</sub>	4.7	< LOD <i>80 (±1)</i>	< LOD <i>0.16 (±0.01)</i>	
SW7	None +O <sub>3</sub>	4.5	< LOD <i>48 (±2)</i>	< LOD <i>0.023 (±0.001)</i>	
IO8	None +O <sub>3</sub>	2.0	14 (±10) <i>2.6 (±1.7)</i>	< LOD <i>0.14 (±0.02)</i>	
SW8	None +O <sub>3</sub>	2.0	14 (±10) <i>2.6 (±1.7)</i>	< LOD <i>0.14 (±0.02)</i>	

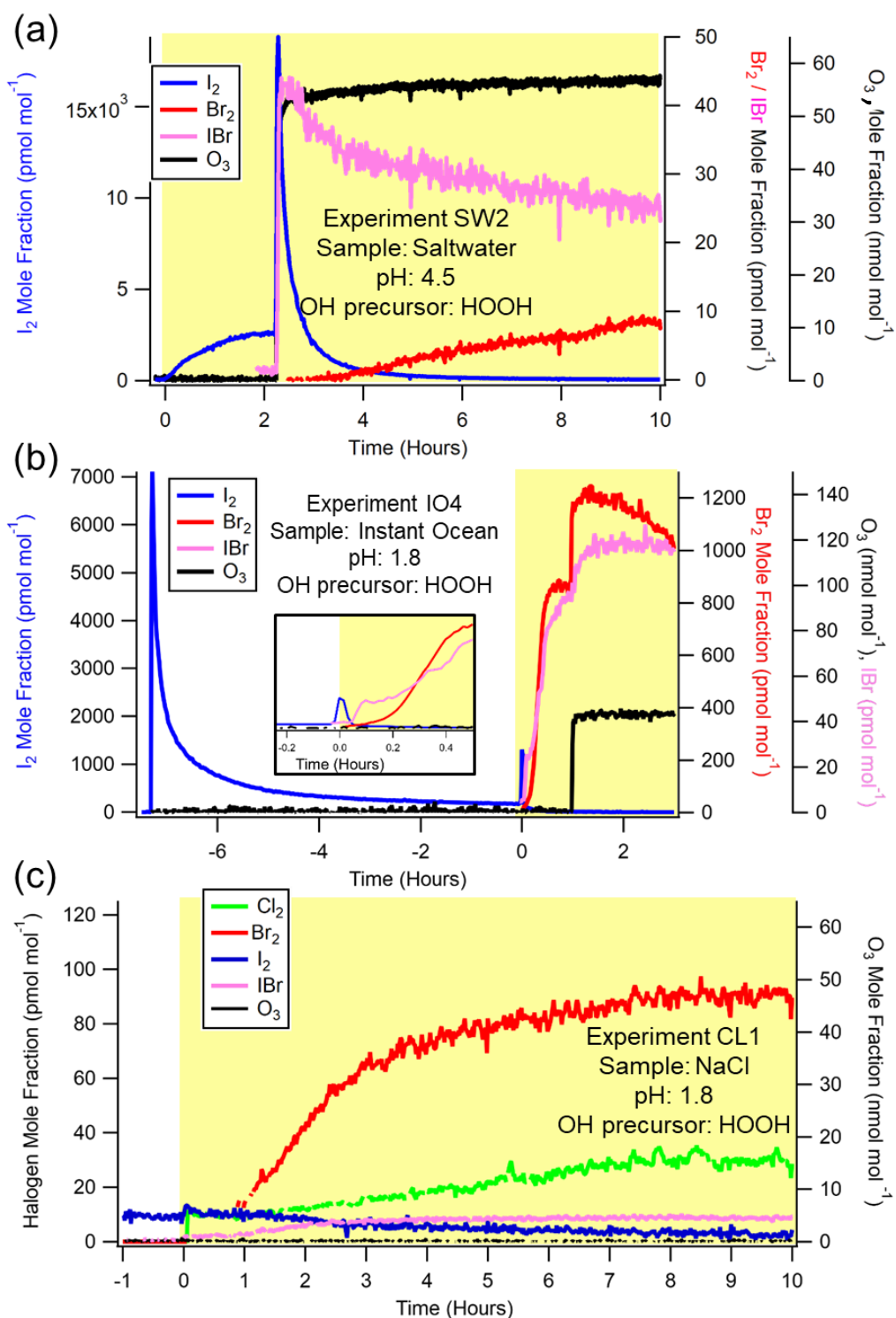
681 **Figures**



682

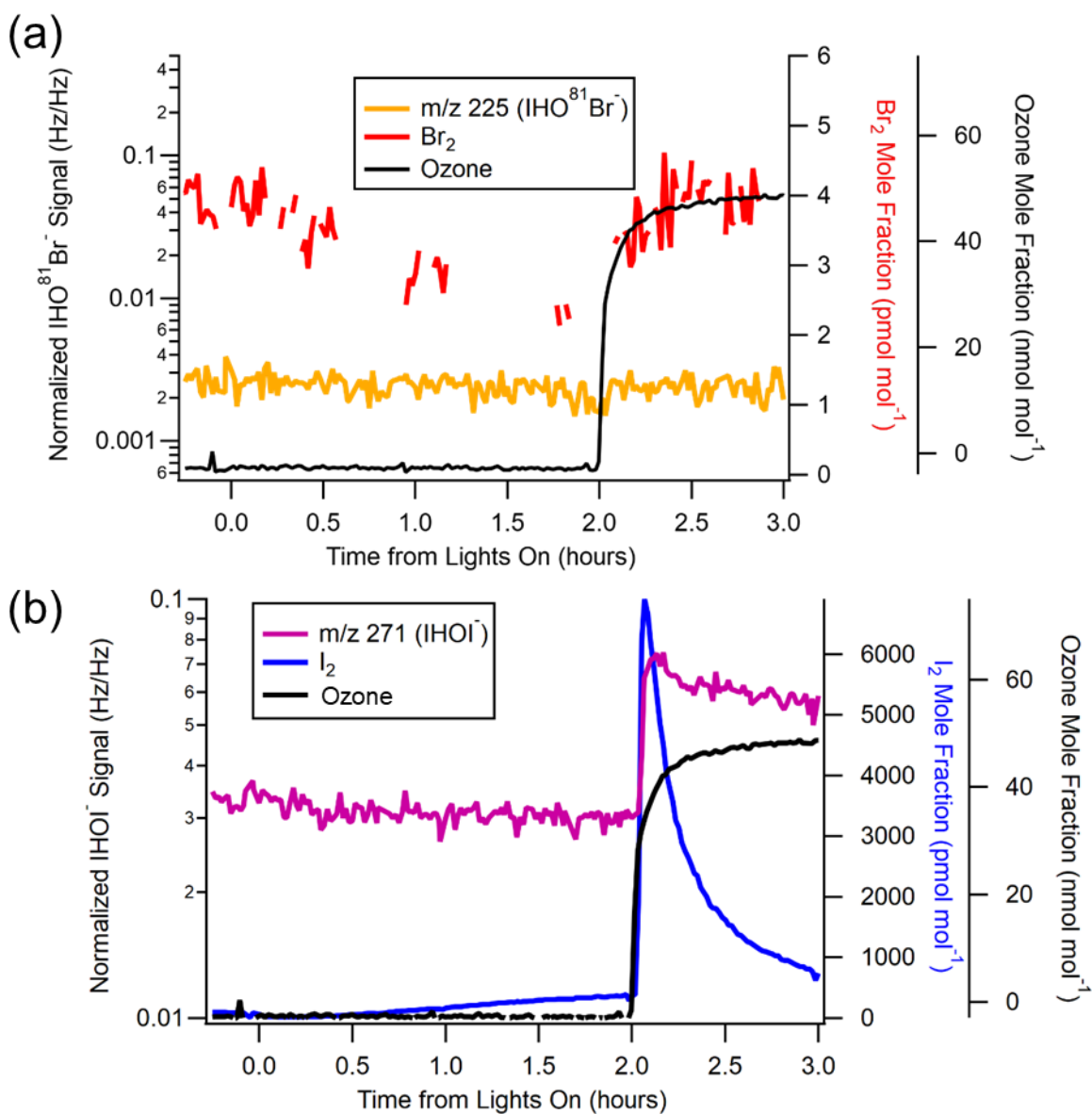
683 Figure 1: Experimental schematic. Purple bars represent powered solar simulator bulbs. The green shading around the flow tube  
684 (flow reactor) represents cooling liquid (60% ethylene glycol, 40% water) circulated through the chiller. The flow reactor region  
685 itself has an inner diameter of 2.5 cm.

686



687

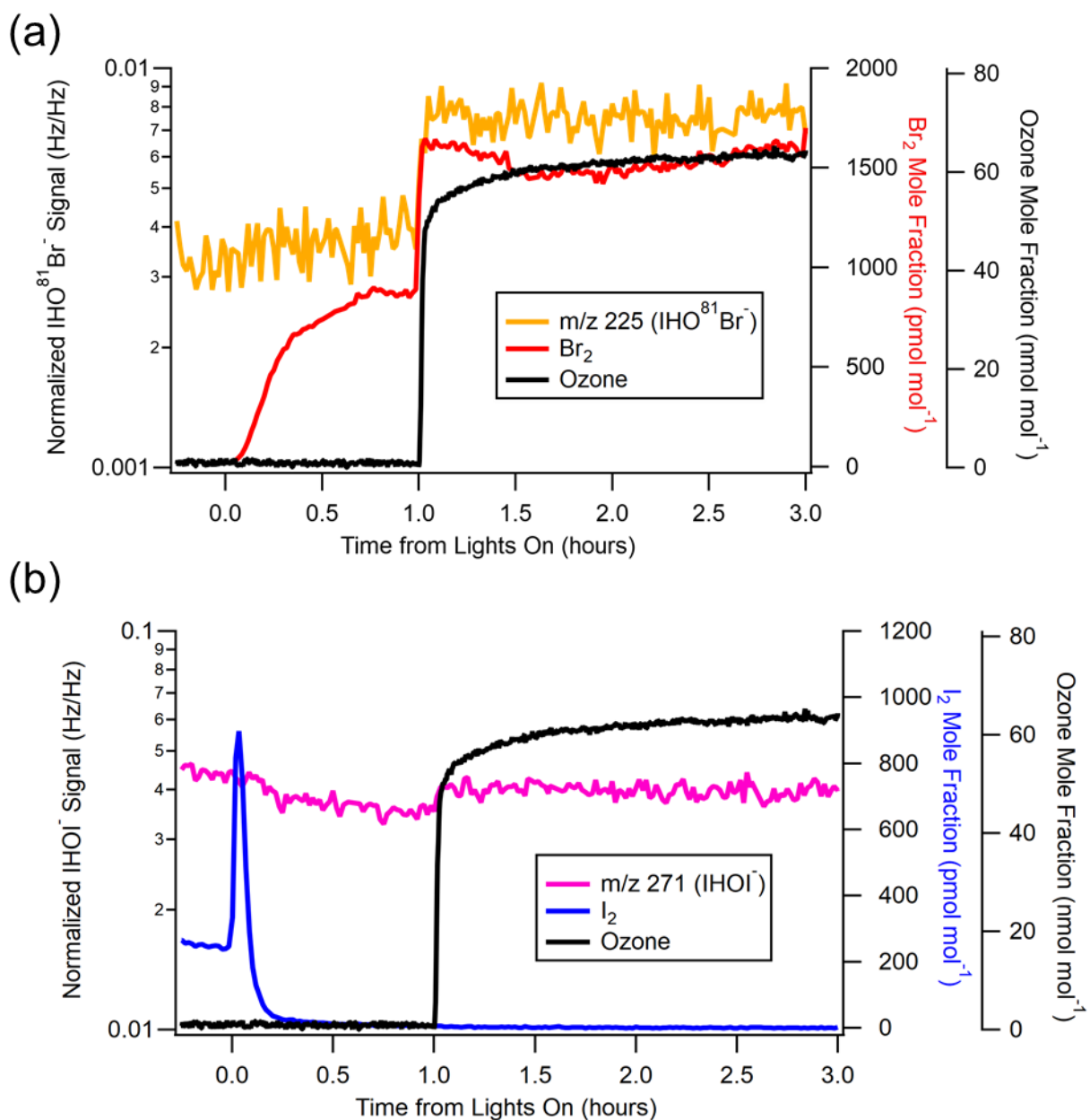
688 Figure 2: Representative experiments of OH-mediated production of  $X_2$ , and subsequent production of  $X_2$  from  $O_3$  addition. a)  
 689 Saltwater experiment (SW2) at pH=4.5. b) Instant Ocean experiment (IO4) at pH = 1.8. Time varying  $Br_2$  and  $IBr$  signals before  
 690  $t=0$  are shown in Fig. S2. Inset more clearly shows the increase of  $I_2$  signal after irradiation. c) NaCl experiment (CL1) at pH = 1.8.  
 691 Timescale represents hours from the activation of the lights, and the yellow shading represents presence of radiation from solar  
 692 simulator bulbs. Gaps in data represent periods when the isotopic ratios showed an interference.



693

694 Figure 3: Normalized, background subtracted HOX signals from experiment IO2, pH=4.7. a) Comparison of  $\text{Br}_2$  mole fractions to  
 695 HOBr ( $m/z$  225). Note that the HOBr signal should be considered only qualitatively as its identity could not be confirmed using  
 696 isotopic ratios with  $m/z$  223 due to its relatively large background signal. b) Effect of  $\text{O}_3$  on  $\text{I}_2$  and HOI.

697



698

699 Figure 4: Normalized, background subtracted HOX signals from experiment SW5, pH=1.8. a) Comparison of  $\text{Br}_2$  mole fractions  
 700 to HOBr ( $m/z$  225). Note that the HOBr signal should be considered only qualitatively as its identity could not be confirmed using  
 701 isotopic ratios with  $m/z$  223. b) Effect of  $\text{O}_3$  on  $\text{I}_2$  and HOI.

702

## 1 2. Methods

### 2 2.1 Materials

3 Acetic acid/acetate and bisulfate/sulfate buffer concentrations were 20 mM (10 mM of each acid and  
4 conjugate base). This concentration was chosen as a compromise between using as little buffer as possible and enough  
5 buffer to ensure adequate buffering ability, as buffer capacity rapidly decreases as constituent species concentrations  
6 approach the acid  $K_a$  value. The halide concentrations from our salt water solutions were  $\text{Cl}^-$  500mM,  $\text{Br}^-$  0.72mM,  
7 and  $\text{I}^-$   $1.9 \times 10^{-3}$  mM.

8 Given that the buffer concentration is comparable to or exceeds halide ion concentrations, there is a concern  
9 that buffer composition may change over time due to the volatility of acetic acid (Henry's Law Constant of 400  
10 M/atm), or because of buffer reactions with OH that may compete with reactions between OH and the halides:



15 Using these aqueous rate constants and the pre-freezing concentrations of species in our paper, we find the following  
16 relative rates of OH-based production:

$$17 \frac{\frac{d[\text{X}_2]}{dt}}{\frac{d[\text{SO}_4^{\cdot-}]}{dt}} = 3.6 \times 10^5, 1.7 \times 10^3, 4.4 \text{ for } \text{Cl}_2, \text{Br}_2, \text{ and } \text{I}_2, \text{ respectively.}$$

$$18 \frac{\frac{d[\text{X}_2]}{dt}}{\frac{d[\text{CH}_3\text{CO}_2\text{H}]}{dt}} = 1.8 \times 10^4, 8.6 \times 10^1, 2.3 \times 10^{-1} \text{ for } \text{Cl}_2, \text{Br}_2, \text{ and } \text{I}_2, \text{ respectively.}$$

19 It is clear based on these relative rates of production that sulfate radical may contribute only a minor amount of Br  
20 and  $\text{Cl}^-$  oxidation in our experiments, less than 0.1% of that from OH-halide oxidation.

21 No comparable rate constant could be found between  $\text{I}^-$  and sulfate.  $\text{I}_2$  production may be impacted by  
22 competition of the  $\text{HSO}_4^-$  and OH. Including dark production, however,  $\text{I}_2$  was consistently our most abundant product  
23 in all experiments except CL1 (in which only trace, undetectable iodide may have been present). Further, we do not  
24 anticipate them occurring to an appreciable degree based on the fact that pH measurements before and after  
25 experiments were identical (indicating no significant depletion of either buffer species throughout the experiment).

26

## 27 2.2 Flow tube

28 Reaction photochemistry was achieved using six UVA-340 solar simulator lamps (Q-Labs, 295 – 400 nm  
29 with maximum wattage at 340 nm, irradiance spectrum in Fig. S1). These lamps were installed in the experiment box  
30 (two on each side, except bottom). Each side was lined with reflective Mylar sheets to evenly irradiate the flow tube  
31 when the lamps were powered.

32

## 33 2.3 CIMS

34 Experiments utilizing the bisulfate/sulfate buffer (IO3-5, IO8, SW3-5, SW8, and CL1) sometimes exhibited  
35 cyclical CIMS signal changes for Br<sub>2</sub> (*m/z* 285, 287, 291), IBr (*m/z* 333, 335) with no attributable cause. These signal  
36 changes occurred seemingly at random and to varying extents. In Fig. S2a, Experiment IO4 (pH = 1.7, includes H<sub>2</sub>O<sub>2</sub>)  
37 demonstrates the most extreme example of this behaviour that almost appears to affect the analysis. First at t = -3, the  
38 Br<sub>2</sub> rises briefly before falling. Then at t=2, the Br<sub>2</sub> signal begins to resemble a sine wave. All data beyond t=2 is not  
39 considered for this specific experiment. In Fig S2b, the effect during Experiment SW5 (pH = 1.7, includes H<sub>2</sub>O<sub>2</sub>) is  
40 more muted, beginning at approximately t = -6 for IBr and Br<sub>2</sub>. As represented by these figures, this behaviour being  
41 farther away from our periods of integration is typical of the remaining experiments. Because these signal changes  
42 occurred outside of the experimental periods analyzed (i.e., before irradiation, and after O<sub>3</sub> had been active for one  
43 hour), they are therefore not believed to affect our results and their interpretation.

44

## 45 3 Results and Discussion

### 46 3.1 Dark reaction production of I<sub>2</sub>

47 In cases without OH precursors at pH < 2, significant photochemical I<sub>2</sub> production still occurs (integrated  
48 production of 14 ± 10 nmol for IO8, and 6.0 ± 2.0 nmol for SW8), while Br<sub>2</sub> and Cl<sub>2</sub> concentrations remain below  
49 limits of detection (consistent with Abbatt et al., (2010), in which no Br<sub>2</sub> was observed without an OH-precursor)  
50 (Table 2, main text). This production likely stems from the mechanisms outlined by Kim et al. (2016) (R13-14, R10-  
51 R12), discussed in the Sect. 1. As discussed in Sect. 3.1, H<sub>2</sub>O<sub>2</sub> or NO<sub>2</sub><sup>-</sup> can react directly with I<sup>-</sup>, thereby reducing the  
52 available [I<sup>-</sup>] for photochemical OH oxidation when pH < 2. When H<sub>2</sub>O<sub>2</sub> was the oxidant, integrated I<sub>2</sub> production

53 amounts were found to be  $\leq 0.82$  nmol (IO4, IO5, and SW5), likely due to this initial dark depletion. When instead  
54  $\text{NO}_2^-$  is used (as in IO3 and SW3), initial amounts of  $\text{I}_2$  on flowtube connection to CIMS were less than when  $\text{H}_2\text{O}_2$   
55 was used (Table S1, Fig. S3). To estimate how much I<sup>-</sup> may have been lost from our frozen sample by these dark  
56 mechanisms, we convert the integrated  $\text{I}_2$  production amounts from Table S1 to I<sup>-</sup> (by multiplying by 2) and subtract  
57 from the maximum possible moles of I<sup>-</sup> in our samples ( $0.0800 \text{ L} * 1.6 \times 10^{-6} \text{ M} = 1.28 \times 10^{-7}$  moles I<sup>-</sup>). For the  
58 samples that use hydrogen peroxide, as little as 36–91% of I<sup>-</sup> is available for reaction, while 94-97% remain when  
59 using  $\text{NO}_2^-$ . However, it is certain that not all of the  $\text{I}_2$  produced by this mechanism went into the CIMS by the nature  
60 of having to break the flow tube seal in order to connect it to the CIMS. Therefore, these are only estimates that could  
61 be affected by the length of time the tube is open to the environment and not connected to the CIMS, or sealed shut.

62

## 63 **3.2 Hydroxyl radical-induced halogen production**

### 64 **3.2.1 pH $\approx$ 4.7**

65 Considering the values of  $\text{I}_2$  production from Table 2 (main text), IO2, appears to have produced  $\sim 10$  times  
66 less  $\text{I}_2$  based on the chosen period of integration. It was noted that  $\text{I}_2$  appeared to already be present within the flow  
67 tube on connecting the flow tube to the CIMS (Fig. S4). The integrated sum of  $\text{I}_2$  released on connection of the flow  
68 tube to the CIMS until stabilization was  $0.8 (\pm 0.1)$  nmol, corresponding to approximately 0.5% of the total 152 nmol  
69 I<sup>-</sup> available for reaction from the Instant Ocean solution (Table S1). This production could possibly be induced by the  
70 dark reactions described in Sect. 3.1. However, the experiment otherwise eventually produces the same qualitative  
71 features as the other three experiments after light activation (Fig. S4). If instead the limits of integration are chosen  
72 starting when the  $\text{I}_2$  signal begins rising (i.e., during a period that qualitatively resembles the other experiments), the  
73 integrated  $\text{I}_2$  production amounts ( $1.1 \pm 0.6$  nmol) more closely approaches analogous experiments (IO1, SW1, SW2).  
74 The apparent photochemical integrated  $\text{Br}_2$  sum of  $0.034 \pm 0.003$  nmol (Table 2) represents a real signal just above  
75 the limit of detection ( $1.8 \pm 0.4$  pmol mol<sup>-1</sup>), but this baseline signal does not change on addition of light (Fig. 3a). In  
76 addition, the integration method used likely interpolated missing data for time periods in which incorrect isotope ratios  
77 between  $m/z$  285 and 287 were observed, thereby overestimating the integrated yield. This signal remains below  
78 limits of quantitation and should not be considered further.  $\text{Cl}_2$  concentrations remained below limits of detection for  
79 experiment IO2.

80 In most cases, it was also found that extending limits of integration beyond 1 h after addition of O<sub>3</sub> did not  
81 produce I<sub>2</sub> in amounts that exhausted the supply of I<sup>-</sup>. In an example experiment (IO2, Fig. S5), the limits of integration  
82 were extended to t = 15 hours after the initiation of lights. While the signal appeared to stabilize below the I<sub>2</sub> LOD of  
83 9 pmol mol<sup>-1</sup>, the calculated I<sub>2</sub> production amount of 70 nmol for this extended integration period only accounts for  
84 46% of the 152 total nmol of I<sup>-</sup> available. When repeated for the other experiments at pH = 4.7, it is found that at least  
85 16% of the original I<sup>-</sup> remains unreacted after similarly extended limits of integration. This suggests that all of the I<sup>-</sup>  
86 in our frozen samples may not be completely excluded to the disordered interface, and may exist within the ice bulk  
87 or inaccessible brine channels throughout the ice, and that differences in integration production amounts can originate  
88 from differences in I<sup>-</sup> distribution during freezing (Bartels-Rausch et al., 2014; Malley et al., 2018).

### 89 3.2.2 pH ≤ 2

90 At low pH (~2), and with H<sub>2</sub>O<sub>2</sub> as our OH precursor, we noted a large outflux of I<sub>2</sub> on connecting the flow  
91 tube to the CIMS. Br<sub>2</sub> production was readily observed in the presence of light, and enhanced when the samples were  
92 exposed to O<sub>3</sub>, as in Fig 2b. However, experiment SW3 (Fig. S5), which was performed with NO<sub>2</sub><sup>-</sup> as the hydroxyl  
93 radical precursor, exhibited photochemical I<sub>2</sub> production on the introduction of radiation. Only after the introduction  
94 of O<sub>3</sub> was Br<sub>2</sub> observed (under proper isotope ratios).

95

### 96 3.3 Effects of O<sub>3</sub> on halogen production

97 As discussed in the main text, HOX compounds were observed when O<sub>3</sub> was added to the flow tube. With  
98 regard to the extent to which it affects our observed signal, we believe volatile organic compounds, such as aldehydes  
99 and ketones, that may form gas phase HX could originate from our cylinder of zero air. However, we believe this  
100 source would be effectively scrubbed by our activated charcoal trap (Fig. 1), mitigating any gas phase production of  
101 HX. There also exists organic matter in the condensed phase, averaging 70 mg/L in each Instant Ocean sample (Sect.  
102 2 of the main text). This carbon-matter is presumably uncharged and would freeze throughout the formed ice (i.e., no  
103 freeze concentration effect), therefore making only a small fraction of the total carbon available at the frozen surface  
104 for reaction.

105 If any of this solution-based carbon were involved in making HX, it would be expected that the SW and IO  
106 experiments produce different amounts of IOHX<sup>-</sup>, given that the SW experiments were found to average ~5 mg/L of

107 dissolved organic matter. However, there is no difference in the signal changes between corresponding SW and IO  
108 experiments (Figs. 3-4, S6). Therefore, we believe the primary source of IOHX<sup>-</sup> in the CIMS is, indeed, HOX formed  
109 in the flow tube.

110

111

## 112 **References**

113 Abbatt, J., Oldridge, N., Symington, A., Chukalovskiy, V., McWhinney, R. D., Sjostedt, S. and Cox, R. A.: Release  
114 of Gas-Phase Halogens by Photolytic Generation of OH in Frozen Halide–Nitrate Solutions: An Active Halogen  
115 Formation Mechanism?, *J. Phys. Chem. A*, 114(23), 6527–6533, doi:10.1021/jp102072t, 2010.

116 Bartels-Rausch, T., Jacobi, H.-W., Kahan, T. F., Thomas, J. L., Thomson, E. S., Abbatt, J. P. D., Ammann, M.,  
117 Blackford, J. R., Bluhm, H., Boxe, C., Domine, F., Frey, M. M., Gladich, I., Guzmán, M. I., Heger, D., Huthwelker,  
118 T., Klán, P., Kuhs, W. F., Kuo, M. H., Maus, S., Moussa, S. G., McNeill, V. F., Newberg, J. T., Pettersson, J. B. C.,  
119 Roeselová, M. and Sodeau, J. R.: A review of air–ice chemical and physical interactions (AICI): liquids, quasi-liquids,  
120 and solids in snow, *Atmos Chem Phys*, 14(3), 1587–1633, doi:10.5194/acp-14-1587-2014, 2014.

121 Malley, P. P. A., Chakraborty, S. and Kahan, T. F.: Physical Characterization of Frozen Saltwater Solutions Using  
122 Raman Microscopy, *ACS Earth Space Chem.*, doi:10.1021/acsearthspacechem.8b00045, 2018.

123 Phibbs, M. K. and Giguère, P. A.: Hydrogen Peroxide and Its Analogues: Iii. Absorption Spectrum of Hydrogen and  
124 Deuterium Peroxides in the Near Ultraviolet, *Can. J. Chem.*, 29(6), 490–493, doi:10.1139/v51-058, 1951.

125

126

127

128

129

130

131

132

133

134

135

136

137

138

139 **Tables**

140 Table S1: Integrated I<sub>2</sub> production amounts prior to irradiation or addition of O<sub>3</sub> from low pH experiments  
141 involving samples with an OH precursor. The period of integration was chosen to be immediately after  
142 connection of flow tube to the CIMS until sample was irradiated. Average LODs for I<sub>2</sub> across experiments  
143 was  $9 \pm 2$  pmol mol<sup>-1</sup>. “IO#” represents samples composed of Instant Ocean, and “SW#” represents  
144 “saltwater” samples, composed of reagent salts.

145

Experiment	Oxidant	pH	I <sub>2</sub> produced (nmol)	Integration time (hours)	Estimated Percent of I <sup>-</sup> remaining for reaction
IO3	NO <sub>2</sub> <sup>-</sup>	2.0	4.0(±0.1)	0.55	93.7
SW4	NO <sub>2</sub> <sup>-</sup>	2.2	2.5(±0.1)	0.43	96.1
SW3	NO <sub>2</sub> <sup>-</sup>	1.8	2.0(±0.1)	0.83	96.8
IO4	H <sub>2</sub> O <sub>2</sub>	1.7	41(±14)	7.28	36.2
IO5	H <sub>2</sub> O <sub>2</sub>	1.7	5.7(±1.9)	2.92	91.1
SW5	H <sub>2</sub> O <sub>2</sub>	1.8	41(±14)	4.95	35.5

146

147

148  
149  
150  
151  
152  
153

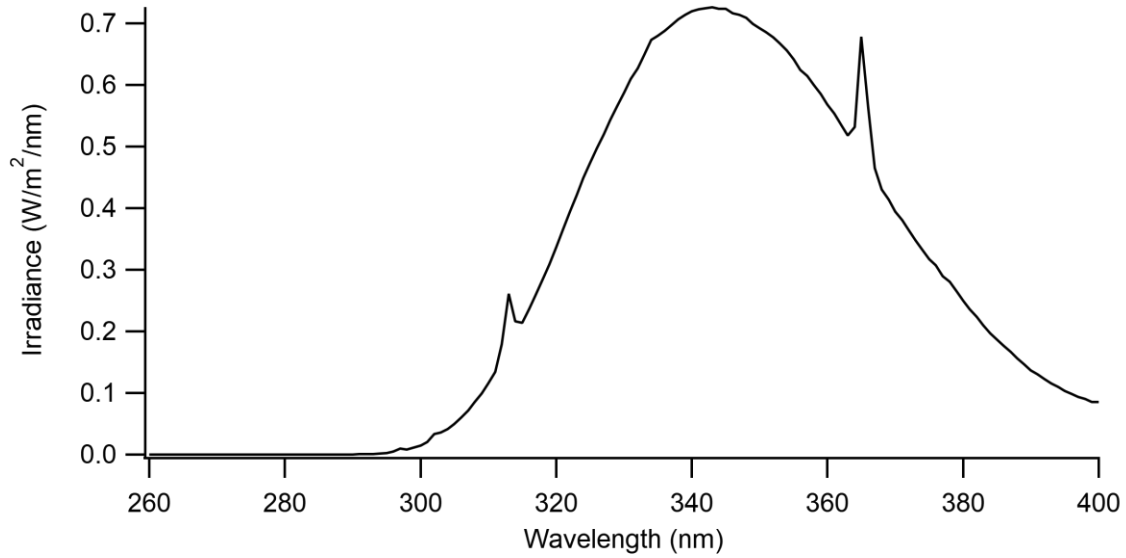
Table S2: Integrated I<sub>2</sub> produced from pH = 4.7 experiments involving samples with an OH precursor. The period of integration begins at sample irradiation and extends past the limits of analysis used in the main text. Average LODs for I<sub>2</sub> across experiments was 9 ± 2 pmol mol<sup>-1</sup>. “IO#” represents samples composed of Instant Ocean, and “SW#” represents “saltwater” samples, composed of reagent salts.

Experiment	Oxidant	pH	I <sub>2</sub> produced (nmol)	Integration time (hours)	Estimated Percent of I <sup>-</sup> remaining for reaction
IO1	H <sub>2</sub> O <sub>2</sub>	4.7	31(±10)	30	59
IO2	H <sub>2</sub> O <sub>2</sub>	4.7	35(±20)	15	54
SW1	H <sub>2</sub> O <sub>2</sub>	4.7	63(±23)	23	17
SW2	H <sub>2</sub> O <sub>2</sub>	4.5	63(±20)	17	16

154  
155  
156

157

158 **Figures**



159

160 Figure S1: Irradiance spectrum for the Q-Lab UVA 340 Lamps, reproduced with permission from Q-Lab  
161 Corporation Technical Bulletin LU-8052 – “SPD for QUV UVA-340.”

162

163

164

165

166

167

168

169

170

171

172

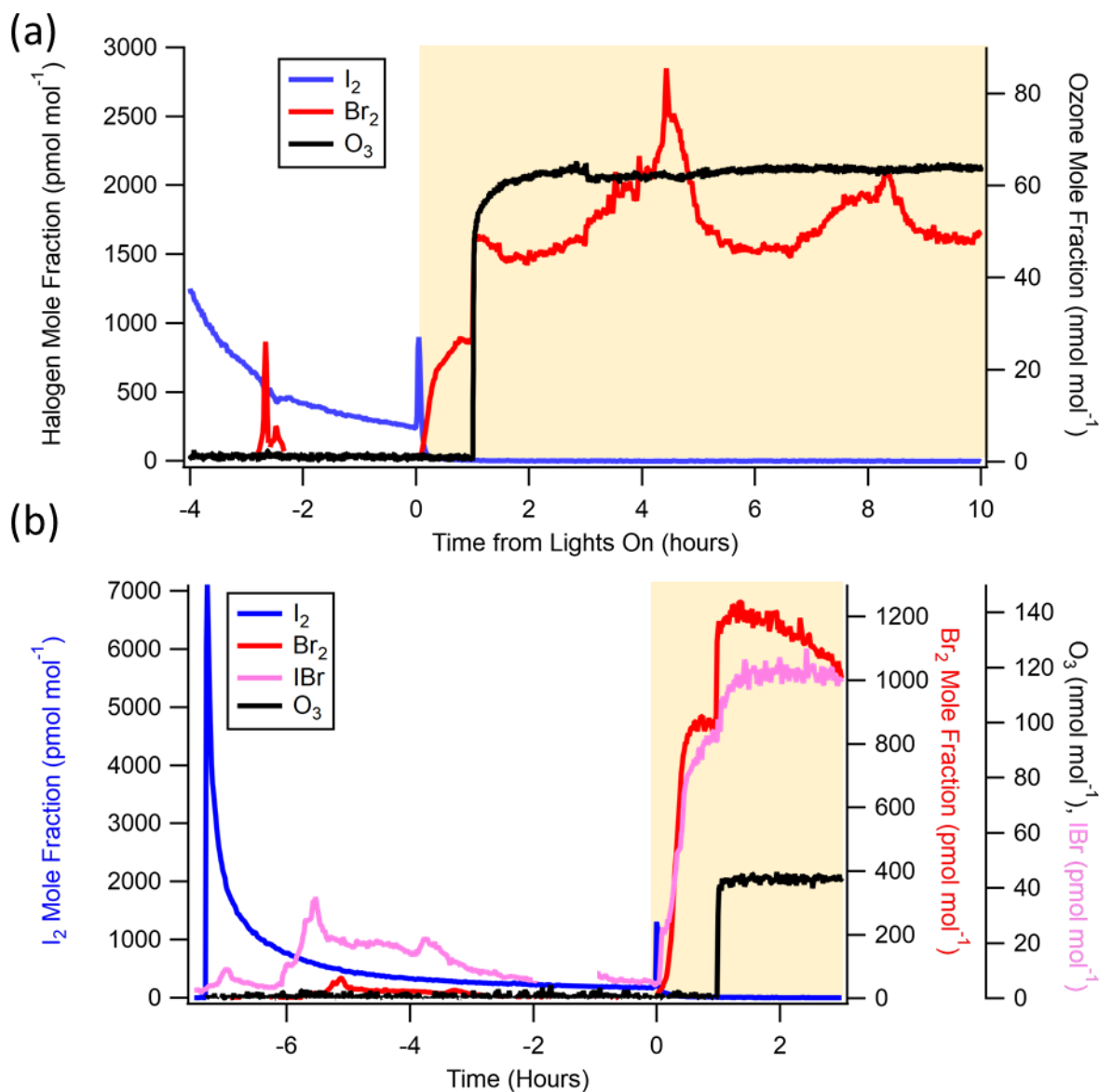
173

174

175

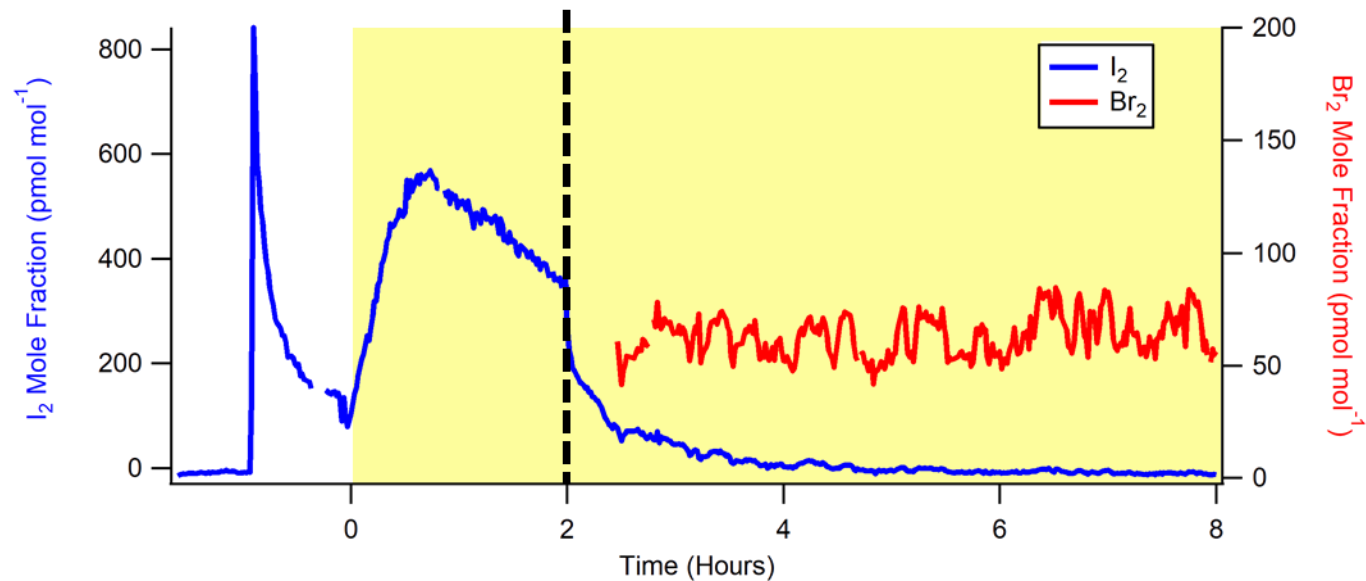
176

177



178  
 179 Figure S2: a) Experiment IO4 (pH < 2, includes H<sub>2</sub>O<sub>2</sub>) time series demonstrating cyclical increases in signal  
 180 Br<sub>2</sub> signals, especially at t = -3 and beginning again at t = 2. Period of analysis in main text includes t = 0  
 181 until t = 2. b) Experiment SW5 (pH < 2, includes H<sub>2</sub>O<sub>2</sub>) time series demonstrating cyclical signals for IBr  
 182 and Br<sub>2</sub>, beginning predominately at t = -6 until shortly before t = 0.

183  
 184  
 185  
 186  
 187

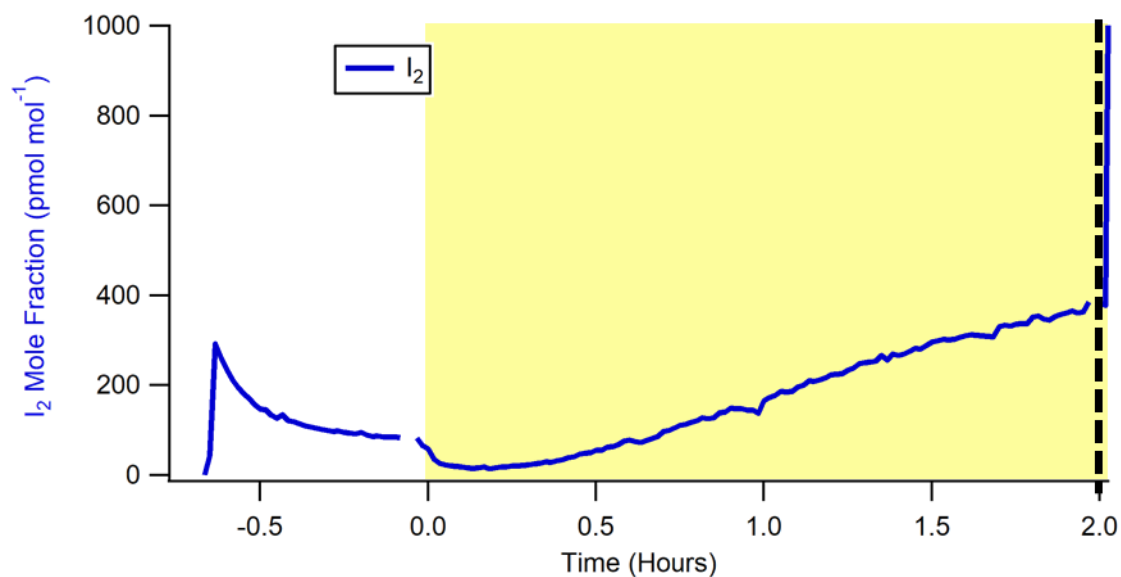


188

189 Figure S3: Experiment SW3, using synthetic seawater at pH = 1.8, in which NO<sub>2</sub><sup>-</sup> acted as our hydroxyl  
 190 radical precursor. Ozone was introduced at hour two (indicated by dashed vertical line), coincident with  
 191 the I<sub>2</sub> concentration decrease. Br<sub>2</sub> data filtered based on correctness of isotope ratios between *m/z* 285 and  
 192 287 (IBrBr).

193

194

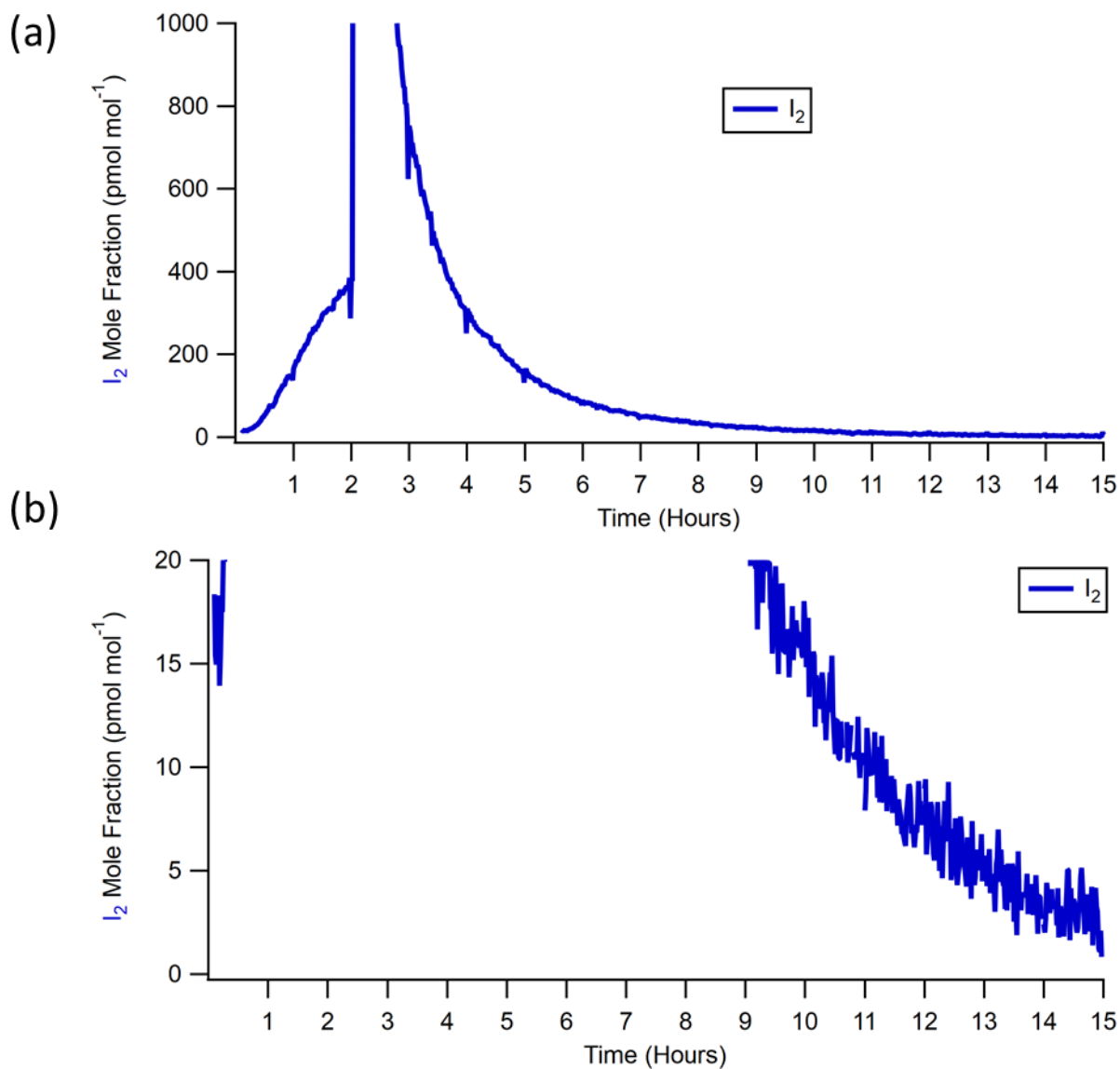


195

196

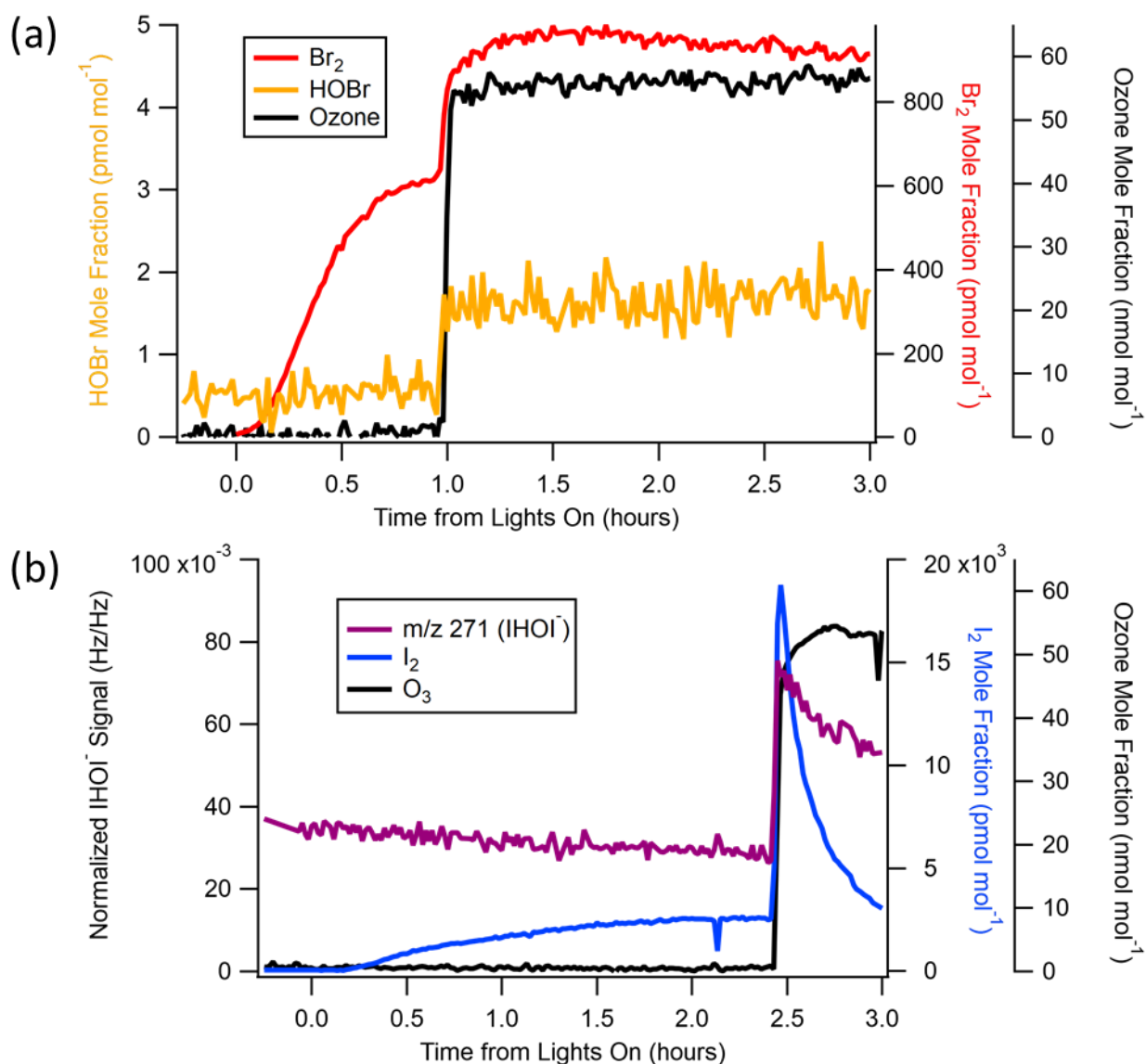
197 Figure S4: Experimental timeseries for experiment IO2. The key difference between this experiment and  
198 others at pH ~4.68 is that there was some initial I<sub>2</sub> present when the flow tube was connected to the CIMS.  
199 On activating the lights, these concentrations lowered, before ultimately rising due to OH-induced I<sub>2</sub>  
200 production. Beginning the integration when the signal begins rising leads to similar production values as  
201 those experiments without this initial I<sub>2</sub> present. Vertical dashed line represents when O<sub>3</sub> was introduced  
202 to the system.

203



204  
 205  
 206  
 207  
 208  
 209  
 210  
 211  
 212

Figure S5: Iodine time series from experiment IO2, using Instant Ocean at pH = 4.7, in which H<sub>2</sub>O<sub>2</sub> acted as our hydroxyl radical precursor. The x-axis begins on light introduction to the flow tube, while ozone was introduced at hour two as indicated by the sudden increase in signal. (a) The time series signal rapidly increases at t=2 coincident with the addition of 60 nmol mol<sup>-1</sup> of O<sub>3</sub>, and then returns to baseline by hour 13. (b) Zoomed in version of the same plot



213

214 Figure S6: a) Experiment IO5, using Instant Ocean at pH = 1.7, in which  $\text{H}_2\text{O}_2$  acted as our hydroxyl radical  
 215 precursor (analogous to SW5, Fig. 4). Comparison of  $\text{Br}_2$  mole fractions to HOBr. Note that the HOBr  
 216 signal should be used only for qualitative purposes as its identity could not be confirmed using isotopic  
 217 ratios with  $m/z$  223 due to its relatively large background signal.  $\text{Br}_2$  data filtered based on correctness of  
 218 isotope ratios between  $m/z$  285 and 287 ( $\text{IBrBr}^-$ ). b) Experiment SW2 (analogous to IO2, Fig. 3) showing  
 219 effect of  $\text{O}_3$  on  $\text{I}_2$  and HOI.

220

221